
Article:
Laib, A., Dahmane, S., Terriche, Y. et al. (3 more authors) (2025) Enhanced automated condition assessment of induction motor bearings: a novel approach using matrix pencil mean frequency signal processing and multilayer perceptron neural networks. IET Electric Power Applications, 19 (1). e70103. ISSN: 1751-8660

https://doi.org/10.1049/elp2.70103

IET Electric Power Applications

WILEY

The Institution of Engineering and Technology

ORIGINAL RESEARCH OPEN ACCESS

Enhanced Automated Condition Assessment of Induction Motor Bearings: A Novel Approach Using Matrix Pencil Mean Frequency Signal Processing and Multilayer Perceptron Neural Networks

Abderrzak Laib[1] | Saida Dahmane[1] | Yacine Terriche[2] | Chun-Lien Su[3] | Hafiz Ahmed[4,5] | Zakaria Chedjara[6]

[1]LGE Research Laboratory, Department of Electrical Engineering, Faculty of Technology, University of M'Sila, M'Sila, Algeria | [2]Ørsted Wind Power A/S, Fredericia, Denmark | [3]Department of Electrical Engineering, National Kaohsiung University of Science and Technology, Kaohsiung City, Taiwan | [4]School of Electrical & Electronic Engineering, University of Sheffield, Sheffield, UK | [5]Autonex Systems Limited, London, UK | [6]Faculty of Applied Sciences, Ibn Khaldoun University of Tiaret Algeria, Tiaret, Algeria

Correspondence: Hafiz Ahmed (hafiz.h.ahmed@ieee.org; hafiz.ahmed@sheffield.ac.uk)

Received: 3 February 2025 | **Revised:** 11 August 2025 | **Accepted:** 8 September 2025

Handling Editor: Huimin Wang

Funding: The authors received no specific funding for this work.

Keywords: fault diagnosis | induction motors | machine bearings | neural nets

ABSTRACT

Vibration signal analysis plays a vital role in the condition-based preventive maintenance of induction motor by identifying early signs of motor issues, avoiding costly breakdowns and optimising the motor's maintenance schedule. It provides detailed information very useful for extending the motor's life cycle with proactive, condition-specific maintenance. Furthermore, the vibration signal analysis offers the advantage of identifying the health status of rotating machinery as a whole, as well as its individual components. This paper presents an innovative solution for the automated health assessment of a critical induction motor component: the bearing. Our approach uses the matrix pencil method for signal processing and health signature generation, combined with a multilayer perceptron neural network to detect health conditions from the resulting health signature characteristics. Initially, the matrix pencil is applied to the vibration signal to identify the mean frequency characteristics. This vector provides a holistic view of the signal's inherent features and transforms its frequency characteristics into a visual spectrum, resulting in improved induction motor bearing fault condition monitoring. Subsequently, the output from the matrix pencil mean frequency analysis is processed by a multilayer perceptron neural classifier, chosen for its low computational cost and high classification accuracy. Experimental validation demonstrates a 100% fault classification rate and automatic identification of defective components. Comprehensive validation further confirms the method's robustness and feasibility for induction motor bearing fault detection compared to other recently methods.

Abbreviations: ANN, Artificial Neural Network; DWT, Discrete Wavelet Transform; EA, Envelope Analysis; EMD, Empirical Mode Decomposition; FFT, Fast Fourier Transform; MLP, Multi-Layer Perceptron; MPM, Matrix Pencil Method; MPMF, Matrix Pencil Mean Frequency; SSA, Singular Spectrum Analysis; SVD, Singular Value Decomposition.

1 | Introduction

Induction motors are essential components in industrial processes, particularly in heavy industry [1], because of their numerous advantages, notably high dependability, low cost, limited maintenance requirements and dynamic performance. Nevertheless, adverse operational environments, such as abrasion, unbalanced loads, or overload can make these motors prone to damage that can disrupt the stator components, rotor and bearing parts. Existing literature show that bearing failure accounts for about 41% of all failures [2] resulting from electrical erosion, inadequate lubrication, vibration damage etc. As such, identifying the bearing failure through condition monitoring is of great importance in ensuring reliable operation of industrial processes.

The development of a predictive approach for fault diagnosis based on precise monitoring can lead to a significant decrease in maintenance costs and machine failure rates [3]. Stator current, noise, temperature, speed, pressure and vibration analysis are some of the physical parameters that can be studied to track failure signs [4–6]. One of the most common ways to detect a bearing problem is through vibration analysis [7]. According to multiple studies, the raw data does not provide anything on the condition of the bearing element, which makes the identification or classification very difficult [8]. Common fault diagnostic techniques have been used in many research, yet they have significant limitations when it comes to complex feature extractions [9, 10]. Intelligent diagnostic techniques can be regarded as a component of knowledge-based approaches and have the ability to automatically learn when combined with artificial intelligence and fault identification methods [11, 12]. In the case of vibration signal analysis, numerous signal processing techniques have been considered for fault identification. The Fast Fourier Transform (FFT) is one of the old techniques that calculates the spectrum of a signal across a wide range of frequencies. However, this approach is not efficient when only a few specific frequencies are considered [13]. The Discrete Wavelet Transform (DWT) and Envelope Analysis (EA) are established methods employed for fault identification, especially in the context of nonstationary signals [14]. The DWT decomposes the original signal, yielding approximations and details that are rich in fault information. The primary limitation of wavelet analysis is its resolution issue, which restricts wavelets to identifying transient signals. The EA provides only the essential information regarding the existence of faults in terms of frequency series. Another extensively studied signal processing technique, the Empirical Mode Decomposition (EMD), is an adaptive tool for signal decomposition and noise reduction, and it can operate on the signal adaptively without requiring prior knowledge about the signal itself. In spite of this, the EMD algorithm has some restrictions, including mode mixing and noise sensitivity. Matrix Pencil Method (MPM), when combined with noise filtering techniques such as Wavelet De-noising and Wiener filtering, has been shown to improve fault detection in noisy environments, as demonstrated in ref. [15]. However, additional comparative analysis with alternative signal processing methods is needed to fully establish its superiority.

In practical cases, the efficacy of the results obtained from the use of the signal processing techniques can only be analysed and evaluated only after the fault occurrence [16]. Additionally, interpreting the results, defining the proper thresholds, using the obtained metrics in the diagnostic process, and regularly monitoring these metrics, all require specialised knowledge [17]. This kind of method adds a human element, which lowers the system's overall fault tolerance. Therefore, efforts are being made to automate the detection process and remove the human element through the use of artificial intelligence [17]. Moreover, accurate fault identification through enhanced feature extraction ultimately improves the system classification performance and reliability.

In view of the literature, many researchers have focused their studies on developing approaches and methods for improving automated bearing faults diagnosis process. In ref. [18], authors have developed an automated diagnosis method for bearing fault identification based on characteristics frequency ratio. Even if this method is automatic, it also requires human involvement for interpreting the obtained results. On the other hand, to improve the efficacy of an intelligent fault diagnosis technique, authors in ref. [19] have used the vibration signals collected in noisy environment conditions as inputs. Then, the authors diagnosed the fault separately by random forest, artificial neural network and autoencoder methods. Results show that autoencoders achieve higher efficiency compared to the other methods. Authors in ref. [20] proposed a condition monitoring process for fault diagnosis of induction motors based on DWT and Artificial Neural Network (ANN) exploiting a current signal. The results show the effectiveness of the proposed method when using the processed signal in the ANN classifier. In summary, utilising raw data without prior signal processing is impractical for big data and fails to yield accurate defect information. Dimensionality reduction is essential, employing various signal processing tools to maintain information integrity.

The key limitations of the existing vibration-based diagnostic approaches identified in the literature can be summarised as follows:

- *Limitations of Raw Data*: Raw vibration data often lacks the necessary detail for accurately identifying and classifying bearing conditions, which complicates the fault diagnosis process. This inadequacy can lead to misinterpretations and missed detections, ultimately hindering effective maintenance strategies.
- *Limitations in Feature Extraction and Signal Processing*: Existing vibration-based diagnostic techniques face challenges in complex feature extraction and exhibit inefficiencies, particularly with traditional methods such as FFT and DWT, which struggle with specific frequencies and resolution issues. Additionally, envelope analysis provides only basic frequency information, lacking comprehensive diagnostic insights.
- *Challenges in Automation and Data Processing*: Current approaches to fault diagnosis face significant challenges, including a reliance on human expertise for interpreting results despite ongoing automation efforts. Additionally, using raw data without prior signal processing proves impractical for large datasets, often leading to inaccurate

defect identification. Effective fault diagnosis necessitates dimensionality reduction and the application of diverse signal processing tools to maintain information integrity.

For this reason, the present paper aims to develop a novel approach that integrates two methodologies to enhance the fault detection and condition monitoring of machinery, particularly focusing on induction motors. Our proposed solution combines signal processing utilising the pencil matrix method with machine learning techniques employing a multilayer perceptron (MLP) neural network. In the first methodology, we introduce the Pencil Matrix method, which separates the machinery vibration signal into frequency vectors, named as Matrix Pencil Mean Frequency (MPMF), enabling the capture of dynamic spectral components. Through careful aggregation, the MPMF emerges as a singular representation, summarising collective frequency characteristics. The resulting MPMF vector not only provides a comprehensive view of the signal's features but also introduces a novel spectrum method, enabling a clearer representation of machinery faults. This approach aims to enhance fault detection and condition monitoring by offering a deeper understanding of the signal's behaviour. Subsequently, a MLP classifier is applied to validate the efficacy of the MPMF as novel features for bearing fault detection. The experiments indicate a high fault classification rate, highlighting the capacity for automatic identification of defective components. The experimental validation conducted with a specialised test rig, alongside comparisons to recent literature, highlights the robustness and practical applicability of the proposed method in real-world scenarios. Our approach advances machinery condition monitoring and fault detection, promising to enhance the reliability and efficiency of industrial systems.

The proposed approach offers several key advantages that address the limitations of existing vibration-based diagnostic techniques:

- *Enhanced Signal Representation*: By employing the Matrix Pencil method, the approach effectively separates machinery vibration signals into frequency vectors, capturing dynamic spectral components. This careful aggregation results in a robust Matrix Pencil Mean Frequency vector that encapsulates collective frequency characteristics, providing a comprehensive view of the signal's features and a clearer representation of machinery faults.
- *Improved Fault Detection and Condition Monitoring*: The integration of the Matrix Pencil method with machine learning techniques enhances fault detection and condition monitoring capabilities, offering a deeper understanding of the signal's behaviour. This holistic analysis enables the identification of potential issues at an earlier stage, thereby improving maintenance strategies.
- *Automatic Fault Classification*: The use of a Multilayer Perceptron classifier validates the effectiveness of the MPMF as novel features for bearing fault detection, demonstrating a high classification rate. This automatic identification of defective components reduces reliance on human expertise and minimises the potential for misinterpretation.
- *Robustness and Practical Applicability*: Experimental validation conducted with a specialised test rig, along with comparisons to recent literature, showcases the robustness and practicality of the proposed method in real-world scenarios. This highlights its potential for effective deployment in industrial settings.
- *Addressing Limitations of Existing Techniques*: The approach effectively overcomes the challenges associated with raw data limitations, inefficient feature extraction, and the need for dimensionality reduction. By integrating advanced signal processing with machine learning, it provides a more reliable and efficient solution for fault diagnosis in induction motors and other machinery.

The structure of the paper is as follows: Section 2 presents an analysis of Matrix Pencil Mean Frequency through the examination of Spectrum Shape. Section 3 provides experimental results and discussions. Section 4 discusses the localisation of the defective component utilising multilayer perceptron neural networks. Section 5 presents a comparative analysis of the proposed method against existing literature. Finally, Section 6 provides a conclusion to the study.

2 | Methodology

2.1 | Matrix Pencil Mean Frequency Analysis via Spectrum Shape

The matrix pencil (MP) method uses a sum of complex exponential to approximate a given dataset, which can be useful to extract different frequency components present in that dataset. Unlike conventional counterparts, MP technique distinguishes itself with its fast computations, precise energy calculations, and its adeptness at extracting various features from the signals. This approach has attracted considerable attention, notably in contexts marked by significant frequency fluctuations, such as shipboard power systems [21, 22]. Here, it proves invaluable for detecting frequency faults, as shown in ref. [23], where the MP is integrated with DWT for detecting frequency-bearing faults during the nonstationary operation of induction motors. Note that Gantmacher introduced the term ‘Pencil’ in 1960 [24] in the context of matrix-values polynomial function.

In our case, the objective is to decompose the measured stator current signal into different frequency components. In this context, the analogue signal $y(t)$ can be approximated as a summation of M damped complex exponential terms, given by the following [25]:

$$y(t) \approx \sum_{i=1}^{M} A_i e^{j\theta_i} e^{(\alpha_i + j\omega_i)t}, \tag{1}$$

where the subscript i indicates the ith component and A, θ, α and ω represent the amplitude, phase, damping factor and angular frequency, respectively. The above continuous-time system can be represented in the discrete-time by using $t = nT_s$ where n is the sampling instant and T_s is the sampling period. In discrete-time, Equation (1) can be rewritten as follows:

$$y(nT_s) = y(n) \approx \sum_{i=1}^{M} A_i e^{j\theta_i} e^{(\alpha_i + j\omega_i)nT_s} = \sum_{i=1}^{M} A_i\, e^{j\theta_i} z_i^n,\ n = 0, 1, ..., N-1, \tag{2}$$

where $z_i = e^{(\alpha_i + j\omega_i)T_s}$ and N is the total number of samples available. In the MP method, the unknown parameters of the ith signal component A, θ and z are estimated from $y(n)$ using a two-step process. In the first-step, the unknown parameter z is estimated using the matrix pencil through solving the generalised eigenvalue problem. As a recap, the generalised eigenvalue problem seeks nontrivial (i.e., nonzero) solutions to $\mathcal{A}\boldsymbol{x} = \lambda\mathcal{B}\boldsymbol{x}$, where $\mathcal{A}$ and $\mathcal{B}$ are matrices, $\boldsymbol{x}$ is a vector and λ is a scalar representing the generalised eigenvalue. In the second-step, using the obtained z, the other unknown parameters A and θ are obtained by solving a least-square problem.

As explained previously, in the first-step, the unknown parameter z is estimated using a mathematical identity known as the matrix pencil and denoted as $\boldsymbol{\mathcal{X}}$, which is a combination of two matrices. From $y(n)$ with length N, the MP is formulated via two matrices, each having a dimension of $(N - L) \times L$, with positive integer L being a tunable MP parameter, as given below:

$$\boldsymbol{\mathcal{X}} = \mathcal{Y}_2 - \lambda\mathcal{Y}_1, \tag{3}$$

where the matrices $\mathcal{Y}_1$ and $\mathcal{Y}_2$ are given by the following equation:

$$\mathcal{Y}_1 = \begin{bmatrix} y(0) & y(1) & \cdots & y(L-1) \\ y(1) & y(2) & \cdots & y(L) \\ \vdots & \vdots & \ddots & \vdots \\ y(N-L-1) & y(N-L) & \cdots & y(N-2) \end{bmatrix}, \tag{4}$$

$$\mathcal{Y}_2 = \begin{bmatrix} y(1) & y(2) & \cdots & y(L) \\ y(2) & y(3) & \cdots & y(L+1) \\ \vdots & \vdots & \ddots & \vdots \\ y(N-L) & y(N-L+1) & \cdots & y(N-1) \end{bmatrix}. \tag{5}$$

Note that L determines the sensitivity of the MP method. As such, L has to be selected as a trade-off between memory requirement, computational complexity and selectivity of the MP method to measurement noise. Using the expression of $y(n)$ from Equation (1), the matrices $\mathcal{Y}_1$ and $\mathcal{Y}_2$ can be rewritten as a function of z and the complex amplitude $R_i = A_i e^{j\theta_i}$ as follows:

$$\mathcal{Y}_1 = \mathcal{Z}_1 \mathcal{R} \mathcal{Z}_2, \tag{6}$$

$$\mathcal{Y}_2 = \mathcal{Z}_1 \mathcal{R} \mathcal{Z}_0 \mathcal{Z}_2, \tag{7}$$

where the matrices $\boldsymbol{\mathcal{R}}$ $(\boldsymbol{M} \times \boldsymbol{M})$, $\boldsymbol{\mathcal{Z}_0}$ $(\boldsymbol{M} \times \boldsymbol{M})$, $\boldsymbol{\mathcal{Z}_1}$ $((\boldsymbol{N} - \boldsymbol{L}) \times \boldsymbol{M})$ and $\boldsymbol{\mathcal{Z}_2}$ $(\boldsymbol{M} \times \boldsymbol{L})$ are given by the following equation:

$$\mathcal{R} = \begin{bmatrix} R_1 & 0 & \cdots & 0 \\ 0 & R_2 & \cdots & 0 \\ \vdots & \vdots & \ddots & \vdots \\ 0 & 0 & \cdots & R_M \end{bmatrix}, \tag{8}$$

$$\mathcal{Z}_0 = \begin{bmatrix} z_1 & 0 & \cdots & 0 \\ 0 & z_2 & \cdots & 0 \\ \vdots & \vdots & \ddots & \vdots \\ 0 & 0 & \cdots & z_M \end{bmatrix}, \tag{9}$$

$$\mathcal{Z}_1 = \begin{bmatrix} 1 & 1 & \cdots & 1 \\ z_1 & z_2 & \cdots & z_M \\ \vdots & \vdots & \ddots & \vdots \\ z_1^{N-L-1} & z_2^{N-L-1} & \cdots & z_M^{N-L-1} \end{bmatrix}, \tag{10}$$

$$\mathcal{Z}_2 = \begin{bmatrix} 1 & z_1 & \cdots & z_1^{L-1} \\ 1 & z_2 & \cdots & z_2^{L-1} \\ \vdots & \vdots & \ddots & \vdots \\ 1 & z_M & \cdots & z_M^{L-1} \end{bmatrix}. \tag{11}$$

Note that in the above formulation, the order of the MP is denoted by $\boldsymbol{M}$. By substituting the Equations (6) and (7) with into the MP definition in Equation (3), the MP can be rewritten as a function of the matrices $\boldsymbol{\mathcal{R}}$, $\boldsymbol{\mathcal{Z}_0}$, $\boldsymbol{\mathcal{Z}_1}$ and $\boldsymbol{\mathcal{Z}_2}$ as follows:

$$\begin{aligned} \boldsymbol{\mathcal{X}} &= \mathcal{Z}_1 \mathcal{R} \mathcal{Z}_0 \mathcal{Z}_2 - \lambda \mathcal{Z}_1 \mathcal{R} \mathcal{Z}_2, \\ \mathcal{Y}_2 - \lambda\mathcal{Y}_1 &= \mathcal{Z}_1 \mathcal{R} (\mathcal{Z}_0 - \lambda\mathcal{I}) \mathcal{Z}_2, \end{aligned} \tag{12}$$

where $\boldsymbol{\mathcal{I}}$ is the identity matrix of dimension $\boldsymbol{M} \times \boldsymbol{M}$. As shown in refs. [24, 26], if the MP tunable parameter L satisfies the condition $\boldsymbol{M} \leq \boldsymbol{L} \leq \boldsymbol{N} - \boldsymbol{M}$, then the MP $\boldsymbol{\mathcal{X}}$ with eigenvalue $\boldsymbol{\lambda}$ has rank M. To show the relationship between $\boldsymbol{z_i}$ (the unknown parameter) and the eigenvalue $\boldsymbol{\lambda}$, the equivalence presented in Equation (12) will be very useful. In this regard, let us consider the term $\boldsymbol{\mathcal{Z}_0} - \boldsymbol{\lambda\mathcal{I}}$, which can be written in the expanded form as follows:

$$\boldsymbol{\mathcal{Z}_0} - \boldsymbol{\lambda\mathcal{I}} = \mathcal{Z}_0 = \begin{bmatrix} z_1 - \lambda & 0 & \cdots & 0 \\ 0 & z_2 - \lambda & \cdots & 0 \\ \vdots & \vdots & \ddots & \vdots \\ 0 & 0 & \cdots & z_M - \lambda \end{bmatrix}. \tag{13}$$

If we consider that $\boldsymbol{\lambda} = \boldsymbol{z_i}, \boldsymbol{i} = \overline{\boldsymbol{1, M}}$, then the $\boldsymbol{i}$-th row of the matrix $\boldsymbol{\mathcal{Z}_0} - \boldsymbol{\lambda\mathcal{I}}$ will become zero, therefore, reducing the rank of the matrix from $\boldsymbol{M}$ to $\boldsymbol{M} - \boldsymbol{1}$. As a result, the rank of the matrix pencil $\boldsymbol{\mathcal{X}} = \boldsymbol{\mathcal{Y}_2} - \boldsymbol{\lambda\mathcal{Y}_1}$ will also reduce to $\boldsymbol{M} - \boldsymbol{1}$ due to the equivalence established by the Equation (13), which implies that $\boldsymbol{z_i}$ becomes generalised eigenvalue of the matrix pair $\{\boldsymbol{\mathcal{Y}_2}, \boldsymbol{\mathcal{Y}_1}\}$ as opposed to ordinary eigenvalues problem. This can be re-casted as an ordinary eigenvalue problem as well if we consider pseudo-inverse of the matrix $\boldsymbol{\mathcal{Y}_1}$. In this case, the eigenvalue problem to estimate $\boldsymbol{z_i}$ can be written as follows:

$$\mathcal{Y}_1^{\dagger}\mathcal{Y}_2 - \lambda\mathcal{I} = 0, \mathcal{Y}_1^{\dagger} = \left(\mathcal{Y}_1^H \mathcal{Y}_1\right)^{-1} \mathcal{Y}_1^H, \tag{14}$$

where Moore–Penrose pseudo-inverse is given by $\boldsymbol{\mathcal{Y}_1^{\dagger}}$ and the superscript $\boldsymbol{H}$ indicates the complex-conjugate transpose. Once the $\boldsymbol{z_i}$'s are obtained, then, the $\boldsymbol{R_i}$'s can be obtained by solving the following least-square problem:

$$\begin{bmatrix} y(0) \\ y(1) \\ \vdots \\ y(N-1) \end{bmatrix} = \begin{bmatrix} 1 & 1 & \cdots & 1 \\ z_1 & z_2 & \cdots & z_M \\ \vdots & \vdots & \ddots & \vdots \\ z_1^{N-1} & z_2^{N-1} & \cdots & z_M^{N-1} \end{bmatrix} \begin{bmatrix} R_1 \\ R_2 \\ \vdots \\ R_M \end{bmatrix}. \quad (15)$$

Note that the matrix pencil method (MPM) and singular spectrum analysis (SSA) [27–32] are both techniques used in signal processing and time series analysis, but they differ significantly in their approach, applications and underlying principles. The MPM is primarily used for estimating the parameters, such as frequencies and damping factors, of exponential signals in the presence of noise and is often applied in areas like modal analysis, system identification, and signal decomposition. MPM models a signal as a sum of damped or undamped exponentials by constructing a Hankel or Toeplitz matrix from the signal, then performing an eigen decomposition of the matrix pencil to estimate the signal's parameters. As a parametric method, MPM assumes a model structure for the signal, involves solving an eigenvalue problem to extract signal parameters, and is commonly applied in scenarios where the signal can be modelled as a sum of exponentials, such as in radar, sonar and vibration analysis.

On the other hand, the SSA is a nonparametric method used for time series decomposition, trend extraction, noise reduction, and identifying underlying structures in data, widely used in fields such as climatology, economics and bioinformatics. SSA involves embedding the time series into a high-dimensional space by constructing a trajectory matrix, which is then subjected to singular value decomposition (SVD), with the resulting components interpreted as trends, oscillatory modes and noise. SSA does not assume any specific model structure for the data, decomposes the time series into components that can be individually analysed, and is useful for exploratory data analysis, signal smoothing, and feature extraction in various time series applications.

In summary, MPM is a parametric method focused on estimating the parameters of exponential components within a signal, often used in structured signal models, while SSA is a nonparametric method aimed at decomposing a time series into interpretable components such as trends and cycles, making it useful for a wide range of exploratory analyses. The choice between these methods depends on the nature of data and the specific goals of analysis.

2.2 | Proposed Approach in Machinery Vibration Signal Analysis for Bearing Faults Identification

The MPM method described above will be used in this Section for analysing vibratory signals of electric machine. The proposed method relies on a six-step approach, as illustrated in Figure 1, to calculate the mean frequency of the vibration signal denoted as matrix pencil mean frequency (MPMF). These steps are as follows:

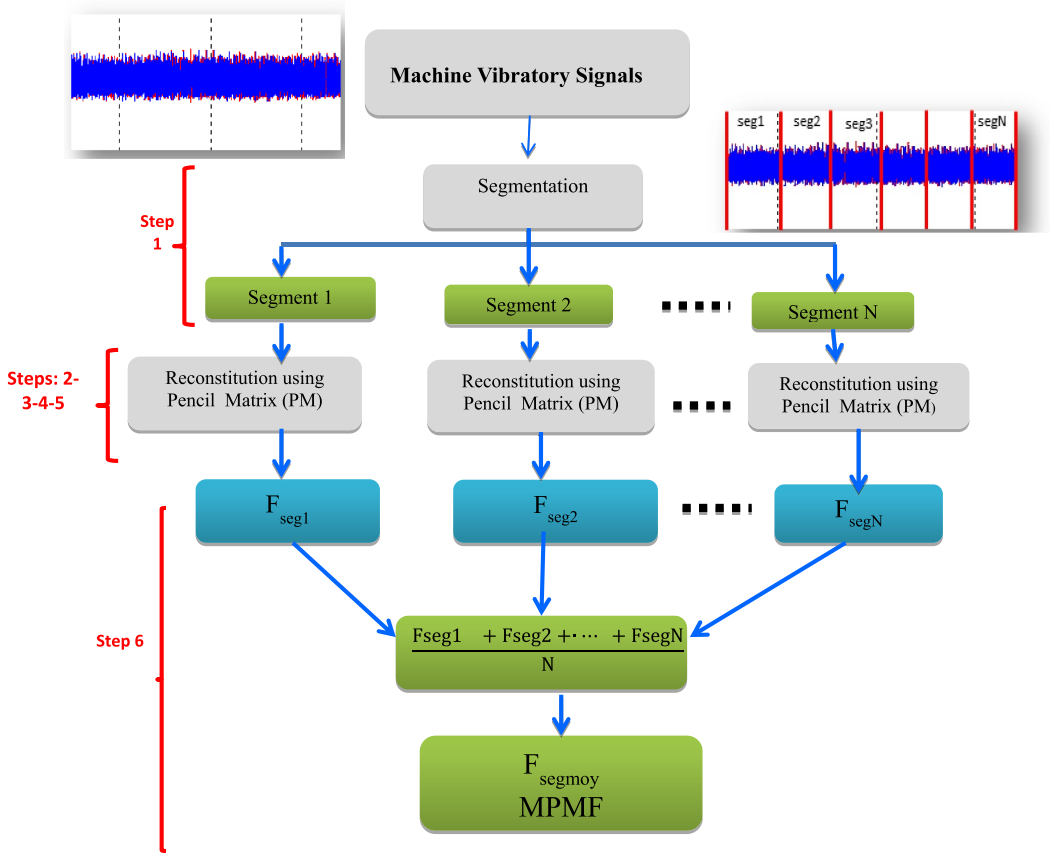

FIGURE 1 | Proposed approach for machinery vibration signal analysis.

- *Step 1: Segmentation Precision*
  It involves the careful segmentation of the machinery vibration signal into several equal length segments. This partitioning serves to focus on specific time intervals and lays the foundation for subsequent in-depth analyses.

- *Step 2: Matrix Pencil Method Selection*
  This step involves the construction of the MP directly from time-domain segments, presenting a departure from conventional frequency-domain transformations like FFT. The essence of this method lies in its recognition that the time-domain can effectively capture unique signal characteristics inherent in machinery vibrations. By leveraging the MP technique, we intricately capture the temporal dynamics, including transient features and nonstationaries, which are often pivotal in machinery health assessments. The careful selection of the MP technique reflects our commitment to a sophisticated analysis that extends beyond conventional approaches.

- *Step 3: Matrix Pencil Method Application*
  Subsequently, each segmented signal (S) undergoes the MP method. This meticulous application yields vectors of frequency for each respective segment, providing a detailed and precise representation of the signal's frequency components. The adaptability of the MP technique to the unique characteristics of machinery vibrations ensures that we capture not only steady-state behaviour but also transient events, enabling a more comprehensive understanding of the machinery's dynamic response.

- *Step 4: Eigenvalue Decomposition:*
  Through eigenvalue decomposition, the MP undergoes a transformation into eigenvalues and eigenvectors. This critical step reveals intrinsic modal frequencies and corresponding vibration modes, offering detailed insights into the complex dynamics of machinery. By incorporating this level of detail, our methodology extends beyond traditional frequency-domain analyses, providing a nuanced understanding of the spatial distribution of vibrational modes.

- *Step 5: Eigenvalue Spectrum Analysis*
  The eigenvalue spectrum serves as a key indicator of machine vibration. Peaks in this spectrum act as pinpointed indicators of dominant frequencies crucial for effective machinery health monitoring.

- *Step 6: Matrix Pencil-based High Precision Mean Frequency Estimation*
  In this final phase, the implementation of the MP method results in a series of frequency vectors, each representing the dynamic spectral components within individual segments of the machinery vibration signal. These vectors offer a detailed portrayal of the signal's frequency dynamics, capturing the nuances of each isolated time frame. To achieve a comprehensive representation of the entire machinery vibration signal, a careful aggregation process takes place. Mean vectors are computed by summing the individual frequency vectors (f) across all segments and dividing the result by the total number of segments. The outcome is a singular frequency vector known as the matrix pencil mean frequency. This vector encapsulates the collective frequency characteristics using the MP approach. This careful averaging technique ensures a balanced consideration of each segment's influence, effectively capturing the underlying characteristics of the entire signal. The resulting MPMF vector provides a holistic view of the machinery vibration signal's inherent features, significantly enhancing the accuracy and resolution of the overall analysis. This aggregation methodology not only synthesises nuanced frequency information across different time intervals but also fosters a more robust understanding of the signal's behaviour. Consequently, it elevates the efficacy of our approach in machinery condition monitoring, fault detection, and predictive maintenance applications.

2.3 | Bearing Fault Frequency Signature

Bearings are critical mechanical components that convert sliding friction into rolling friction to minimise losses and consist of an inner ring (ir), outer ring (or), rolling elements (re) and a cage (c) (cf. Figure 2a,b). The inner ring rotates with the shaft, while the outer ring supports the assembly, and the cage distributes the rolling elements. Note that in Figure 2a, the diameter of the rolling element is denoted by $\boldsymbol{d}$, while the diameter of the bearing pitch is denoted by $\boldsymbol{D}$ and $\boldsymbol{\alpha}$ is the operating angle of the bearing (0° for ball bearing). Additionally, $\boldsymbol{n_b}$ denotes the total number of rolling elements (spheres). Common faults can occur on the inner race, outer race, cage and rolling elements. Frequencies related to these faults are denoted as $\boldsymbol{f_{ir}}, \boldsymbol{f_{or}}, \boldsymbol{f_c}$ and $\boldsymbol{f_{re}}$, respectively while the motor rotational frequency is denoted by $\boldsymbol{f_r}$ and given by $\boldsymbol{f_r = n/60}$ with $\boldsymbol{n}$ being the motor rotational speed. Theoretical fault frequencies for these components [33, 34] are given below.

- *Inner ring defect characteristic frequency*: the distinctive vibration frequency caused by faults in the inner, also known as 'bearing pass frequency of inner race' is calculated using the following formula:

$$f_{\mathrm{ir}} = \frac{n_b}{2} f_{\mathrm{r}} \left(1 + \frac{d}{D} \cos \alpha\right). \tag{16}$$

- *Cage defect characteristic frequency*: the cage is attached between the inner ring and the outer ring; this attachment generates defects that can be expressed by the following equation:

$$f_{\mathrm{c}} = \frac{1}{2} f_{\mathrm{r}} \left(1 \pm \frac{d}{D} \cos \alpha\right). \tag{17}$$

- *Rolling element defect characteristic frequency*: the ball makes contact between the inner and outer rings, resulting in a fault at the contact point, as represented by the following equation:

$$f_{re} = \frac{D}{d} f_r \left(1 - \left(\frac{d}{D}\cos\alpha\right)^2\right). \quad (18)$$

- *Outer ring defect characteristic frequency*: the outer ring is immobile, so the fault can occur through the passage of a ball, which is known as 'the bearing pass frequency of outer race' and is calculated using the following formula:

$$f_{or} = \frac{n_b}{2} f_r \left(1 - \frac{d}{D}\cos\alpha\right). \quad (19)$$

2.4 | Bearing Element Dynamics: Experimental Setup

The data sets that were utilised in the present work include the vibration signals generated from the bearings and gathered from the test rig of the Case Western Reserve University (CWRU) [35]. The test rig, as illustrated in Figure 3, consists of a 1.5 kW asynchronous motor that transfers a load via a shaft that is connected to the motor. On this shaft, an encoder and torque transducer are mounted to ensure precise data collection for speed and torque. Following this, accelerometers are connected to the motor housing through its magnetic base to gather vibration signals at a sampling frequency of 12 kHz.

Motor loads can be controlled via variable frequency drives in direct correlation to torque delivered, all thanks to the control unit. Thus, a rise in torque and a fall in shaft speed are the outcomes of increasing the motor load. The experiments are carried out with four different loads used to generate the vibratory signals: 0, 1, 2 and 3 Nm, and under four different motor speeds, which correspond to 1797, 1772, 1750 and 1730 revolutions per minute, respectively. Although the test bearings were being subjected to the creation of single-point flaws by the application of electro-discharge machining, the bearings were also being damaged. The flaws were distinguished by their varied sizes, especially 0.007, 0.014, 0.021 and 0.028 inch (corresponding to 0.1778, 0.3556, 0.5334 and 0.7112 mm) based on their dimensions.

About 64 cases of bearings that were fitted in the drive end were found to be normal and faulty, according to the data sets that included vibration signals. Four of these cases are issued under normal conditions, while the remaining data sets are acquired from defective bearings, comprising 28 faulty cases in the outer race. Among these, 12 cases of them are associated with a fault diameter of 0.007 inches, 4 with a fault diameter of 0.014 inches,

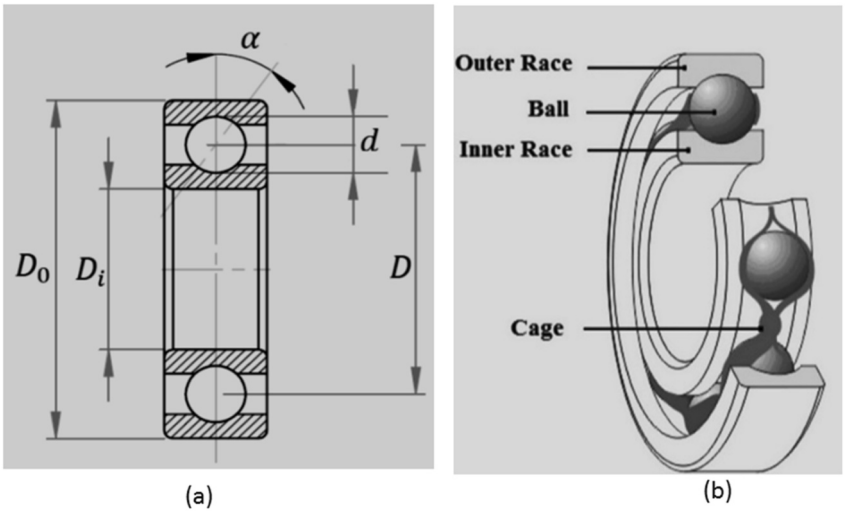

FIGURE 2 | (a) Overall rolling bearing structure. (b) Geometric properties of the bearing.

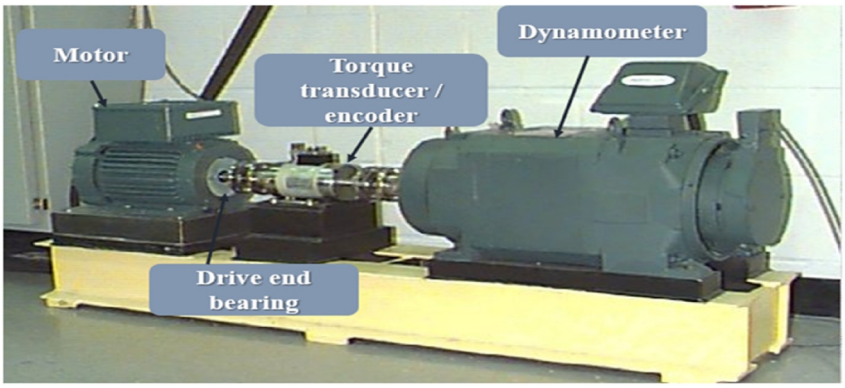

FIGURE 3 | Experimental test rig for the operation of CWRU bearings [35].

and 12 with a fault diameter of 0.021 inches. Therefore, a defective bearing with a rolling element comprises 16 faulty cases, with each 4 of them corresponding to fault diameters of 0.007, 0.014, 0.021 and 0.028 inches, respectively. Additionally, a defective bearing with a Haut du formulaire inner race fault includes 16 faulty cases, divided into 4 cases corresponding to fault diameters of 0.007, 0.014, 0.021 and 0.028 inches, in which each bearing condition's bearing data is provided in a unique Matlab file. Table 1 provides a listing of the characteristics of the bearings that were utilised in this study.

3 | Experimental Results and Discussions

3.1 | Enhancing Reconstitution Machinery Vibration Signals Through Matrix Pencil Analysis

Figures 4–7 present a comprehensive analysis of vibratory signatures and reconstituted signals utilising the pencil matrix method across diverse scenarios: a healthy bearing, a bearing with a rolling element fault, a bearing with an inner race fault, and a bearing with an outer race fault. The study focuses on a no-load motor example with a fault diameter of 0.1778 mm. In detail, Figure 4 showcases the faithfully reproduced vibratory signatures of a healthy bearing using the MP method with $M = 100$ poles and SL = 250.

Figure 5 captures the reconstituted vibratory signatures of a bearing with a rolling element fault (Ball), also employing MP with $M = 100$ poles and SL = 250. Likewise, Figure 6 depicts the reproduced vibratory signatures of a bearing with an inner race fault, and Figure 7 illustrates the reproduced vibratory signatures of a bearing with an outer race fault, both utilising MP with $M = 100$ poles and SL = 250. These findings, consistently derived with a minimal number of poles ($M = 100$) and a segment length (SL = 250), underscore the method's reliability in faithfully reproducing original vibratory signatures across diverse conditions, including healthy bearings, and those with outer race faults, rolling element faults and inner race faults.

TABLE 1 | SKF ball bearings specifications for 6205-2RS JEM.

Bearing elements	Dimensions
Inside diameter	25 mm
Outside diameter	52 mm
Intermediate diameter	39 mm
Thickness	15 mm
Rolling element diameter	8 mm
Rolling element number	9
Contact angle	rad

3.2 | The Matrix Pencil Mean Frequency Reconstitution Results

Implementing the MP method reveals dynamic spectral components in machinery vibration signals, offering detailed frequency dynamics within individual segments. Through meticulous aggregation and mean vectors form the MPMF, it provides a holistic view of the signal's inherent characteristics. This refined methodology enhances accuracy, resolution, and understanding of machinery behaviour, contributing to improved condition monitoring, fault detection and predictive maintenance.

In this study, we utilised the CWRU bearing dataset, which provides standardised vibration signals for fault diagnosis. The faults in the dataset were artificially induced using electrical discharge machining to ensure high precision and consistency in both location and shape across different fault types. This controlled fault induction process minimises variations that could otherwise introduce inconsistencies in the extracted features.

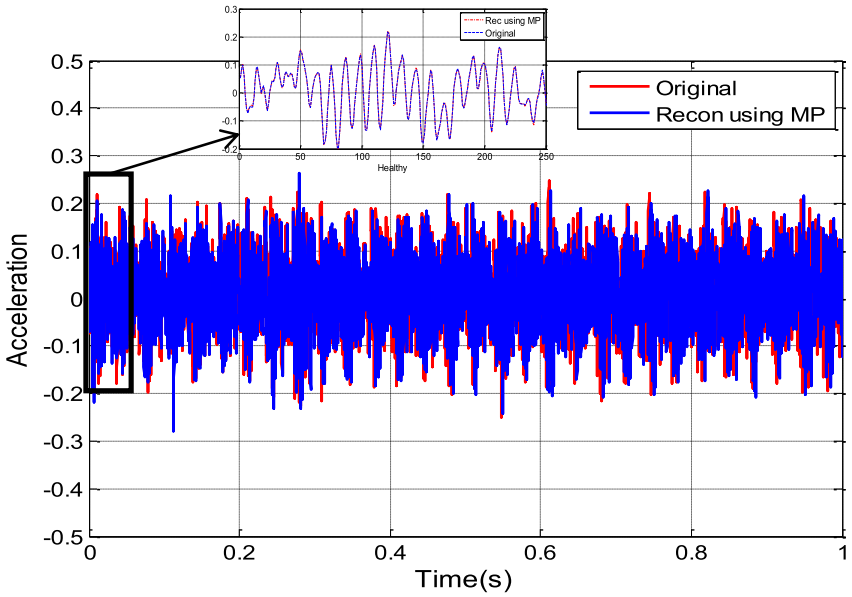

FIGURE 4 | Reproduced vibratory signatures of healthy bearing using MP with $M = 100$ poles and SL = 250.

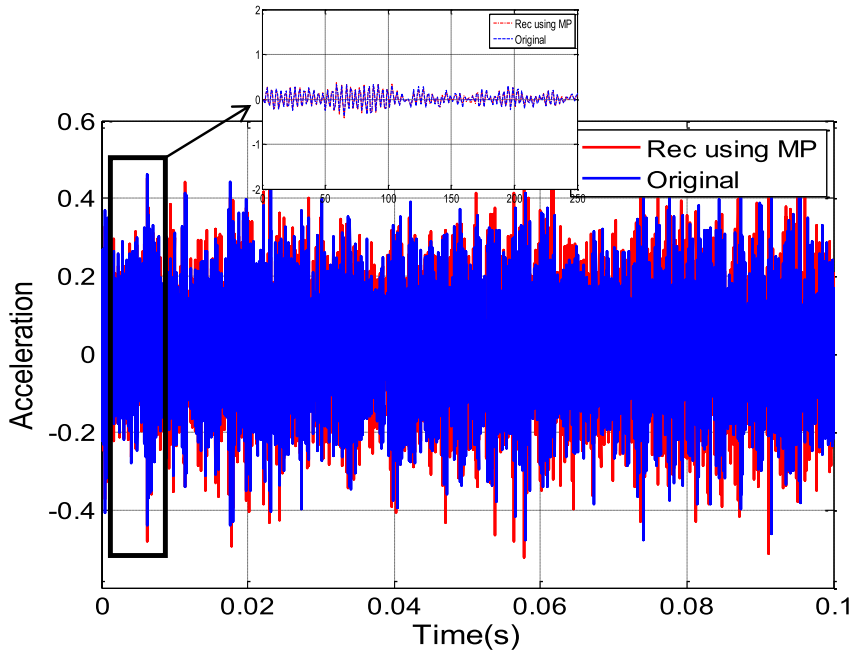

FIGURE 5 | Reproduced vibratory signatures of bearing with a rolling element fault (ball) using MP with $M = 100$ poles and SL = 250.

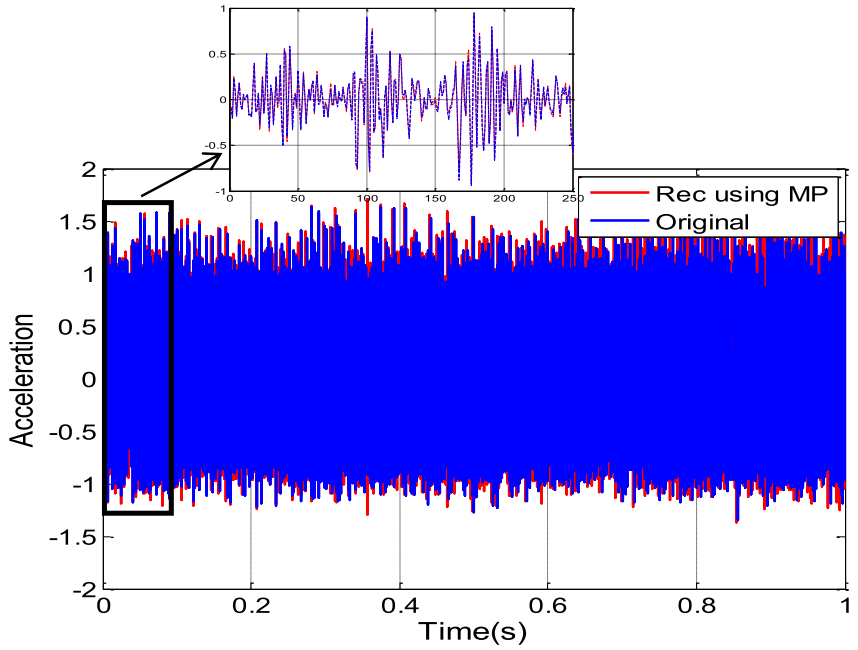

FIGURE 6 | Reproduced vibratory signatures of bearing with an inner race fault using MP with $M = 100$ poles and SL = 250.

The dataset includes bearing defects in three distinct locations: rolling elements, inner race and outer race, with predefined fault diameters of 0.007, 0.014, 0.021 and 0.028 inches. Because all faults of a given type and size were introduced under the same conditions, the vibrational response primarily reflects the mechanical behaviour of the faults rather than uncontrolled variations in flaw geometry or placement.

Additionally, the CWRU test rig maintains controlled operating conditions, such as rotational speed and load, ensuring that the recorded vibration signals are not influenced by external variations. This consistency allows us to analyse the effectiveness of the MPMF method in differentiating fault severities based on intrinsic signal characteristics rather than uncontrolled experimental factors. By leveraging this standardised dataset, our study ensures that fault classification is based on robust spectral differences captured by the MPMF approach, rather than artefacts introduced by inconsistent flaw placement or shape variations.

The approach marks a substantial advancement in comprehending machinery health and performance. Figure 8 presents the results of MPMFs for a healthy bearing state. The original database consists of four distinct healthy bearing vibration

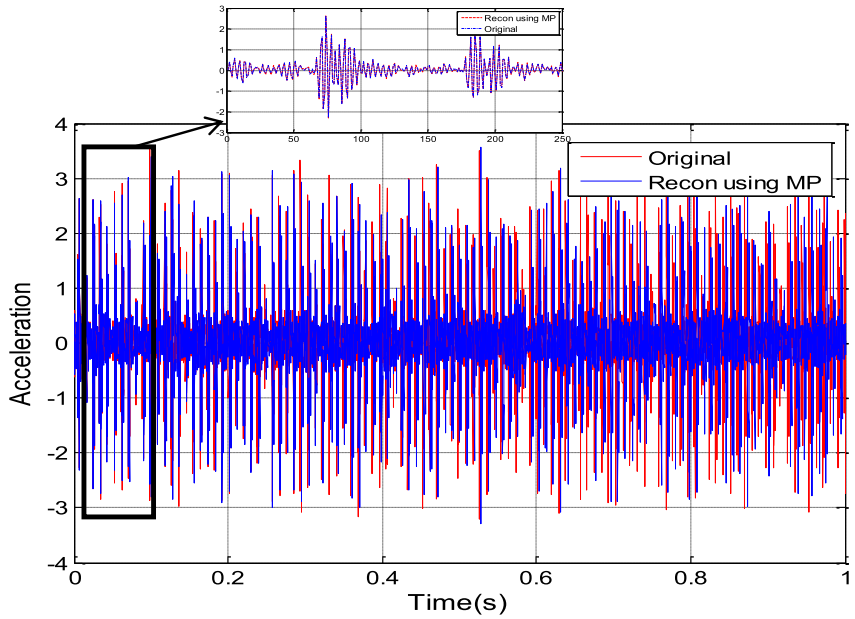

FIGURE 7 | Reproduced vibratory signatures of bearing with an outer race fault using MP with $M = 100$ poles and SL = 250.

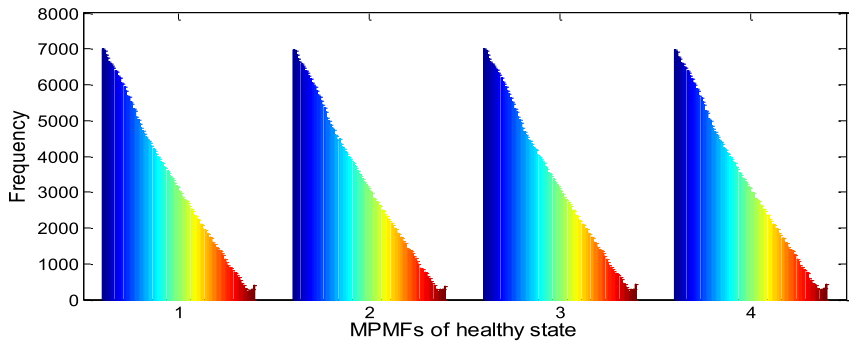

FIGURE 8 | Matrix pencil mean frequency of healthy bearing.

signals, each reconstructed using our proposed approach based on MP with a minimal number of poles ($M = 100$) and a segment length (SL = 250). Each MPMF encapsulates the inherent characteristics of each healthy bearing vibration signal. The colour spectrum, transitioning from blue to red, represents the frequencies of the 100 poles, ranging from 1 to 100 poles. Notably, a clear similarity in MPMF forms emerges, highlighting the consistency across these signals.

Figure 9 illustrates the second case of MPMFs for bearings exhibiting faults in the rolling elements. The original database comprises 16 distinct vibration signals from bearings exhibiting faults in the rolling elements, each reconstructed using our proposed MP approach with a minimal number of poles ($M = 100$) and a segment length (SL = 250). Each MPMF captures the intrinsic characteristics of the vibration signal associated with a bearing exhibiting rolling element faults. The colour spectrum, transitioning from blue to red, represents the frequencies of the 100 poles, ranging from 1 to 100 poles. Notably, a pronounced resemblance in the forms of the first 4 MPMFs emerges, emphasising the consistency across these signals, exemplified by bearings with a rolling element fault diameter of 0.007 inches. This pattern of similarity extends to MPMFs 5–8, which correspond to bearings with rolling element faults measuring 0.014 inches and persists in the subsequent MPMFs (9–12 and 13–16) corresponding to bearings with rolling element faults of 0.021 and 0.028, respectively. A closer examination of the MPMF structures reveals clear differences in the higher-order poles (represented by red colours) between the 0.007 and 0.014-inch faults. Specifically, MPMFs 1–4 correspond to the 0.007-inch fault, while MPMFs 5–8 represent the 0.014-inch fault. These variations indicate the more pronounced mechanical impact of larger defects on the rolling elements, leading to stronger fault-related frequency components in the vibration signal. The consistent differentiation observed across fault diameters in Figure 9 further reinforces the effectiveness of MPMF in capturing and distinguishing fault severity. The MPMF shapes effectively capture and differentiate the vibrational characteristics associated with fault diameter for bearings with a rolling element fault.

Figure 10 depicts the third scenario of Matrix Pencil Mean Frequency (MPMFs) for bearings with an inner race fault. The original dataset consists of 16 distinct vibration signals from bearings with an inner race fault, each reconstructed using the

proposed Matrix Pencil approach with a minimal number of poles ($M = 100$) and a segment length (SL = 250). Each MPMF captures the inherent characteristics of the corresponding bearing with an inner race fault vibration signal. The colour spectrum, transitioning from blue to red, represents the frequencies of the 100 poles, ranging from 1 to 100 poles. Significantly, a distinct resemblance in the forms of the first four MPMFs emerges, highlighting the consistency across these signals, illustrated by bearings with an inner race fault diameter of 0.007″. This consistent pattern extends to MPMFs 5–8, reflecting bearings with an inner race fault of 0.028″, and persists in the subsequent MPMFs (9–12 and 13–16), corresponding to bearings with inner race faults of 0.014 and 0.021, respectively. The MPMF shapes successfully capture and distinguish the vibrational characteristics associated with fault diameter for from bearings with an inner race fault.

Figure 11 illustrates the fourth scenario of MPMFs for bearings showing an outer race fault. The original dataset comprises 28 distinct vibration signals from bearings with an outer race fault, each reconstructed using the Matrix Pencil approach with a minimal number of poles ($M = 100$) and a segment length (SL = 250). Each MPMF encapsulates the unique characteristics of the corresponding bearing with an outer race fault vibration signal. The colour spectrum, transitioning from blue to red, represents the frequencies of the 100 poles, ranging from 1 to 100 poles. A noticeable distinction in the forms of the first four MPMFs emerges, emphasising the consistency across these signals, exemplified by bearings with an outer race fault diameter of 0.014″. This distinctive pattern extends to MPMFs 5–8, 9–12, 13–16, reflecting bearings with an outer race fault of 0.07 under different accelerometer positions (centred for MPMFs 5–8, opposite for MPMFs 9–12, orthogonal for MPMFs 19–16),

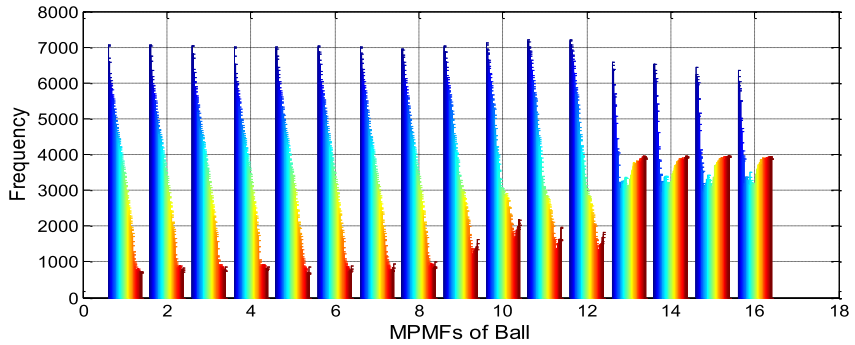

FIGURE 9 | Matrix pencil mean frequency of bearing with a rolling element fault (ball).

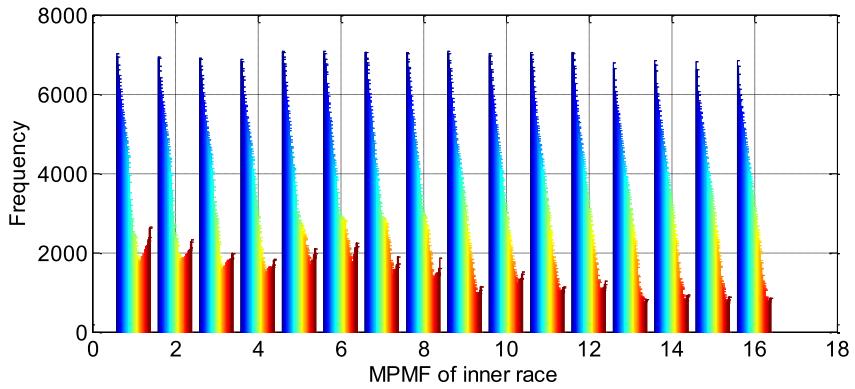

FIGURE 10 | Matrix pencil mean frequency of bearing with an inner race fault.

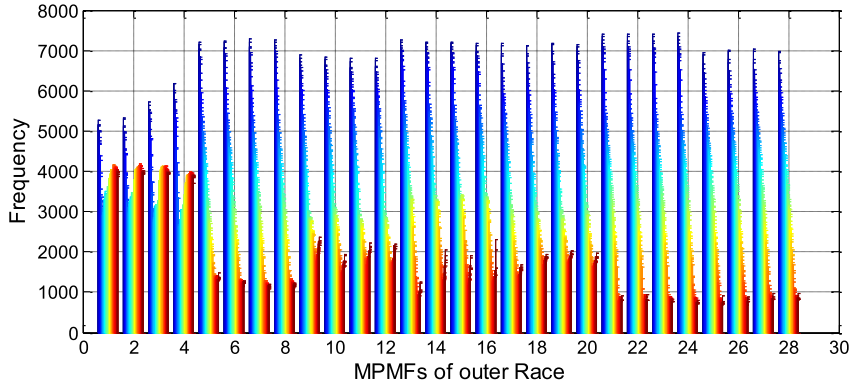

FIGURE 11 | Matrix pencil mean frequency of bearing with an outer race fault.

and persists in the subsequent MPMFs (17–20, 21–24, 25–28), corresponding to bearings with outer race faults of 0.021″ under different accelerometer positions (centred for MPMFs 17–20, opposite for MPMFs 21–24, orthogonal for MPMFs 25–28). The MPMF shapes efficaciously capture and discriminate the vibrational characteristics linked with fault diameter for bearings with an outer race fault.

Figure 12 illustrates examples of the MPMF shapes corresponding to different bearing conditions: the first depicts the MPMF spectrum shape of a healthy bearing, the second portrays a bearing with an inner race fault, the third displays a bearing with an outer race fault, and the fourth represents a bearing with a rolling element fault. Each type of fault exhibits a distinct format, serving as a unique representation of its fault type. These MPMF profiles adeptly capture and distinguish the vibrational characteristics associated with various bearing conditions.

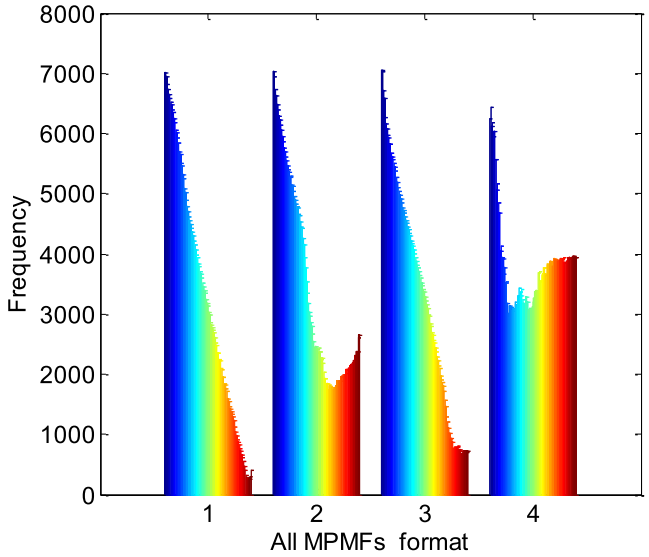

FIGURE 12 | Examples of all MPMF formats.

3.3 | Exploring the Impact of Number of Poles on the Forms of MPMF

3.3.1 | For Bearing Inner Race

Figure 13 clearly illustrates the impact of varying the number of poles (M) on the formats of MPMFs for bearings exhibiting an inner race fault. The dataset comprises 16 distinct vibration signals from bearings with an inner race fault, each reconstructed using the proposed MP approach with different numbers of poles: $M = 70$, $M = 50$, and $M = 30$. The colour spectrum, transitioning from blue to red, represents the frequencies of the poles for each case ($M = 70$, $M = 50$, $M = 30$). The effect of the variation in the number of poles is evident as the format of MPMF changes for each case. Notably, the variation in bearings with an inner race fault diameter of 0.007″ is most pronounced in the first four MPMFs. This consistent pattern extends to MPMFs 5–8, reflecting bearings with an inner race fault of 0.028″, and persists in the subsequent MPMFs (9–12 and 13–16), corresponding to bearings with inner race faults of 0.014″ and 0.021″, respectively. These distinct resemblances in the forms of the MPMFs highlight the consistency across these signals. The shapes of the MPMFs effectively capture and distinguish the vibrational characteristics associated with different numbers of poles for bearings with an inner race fault.

3.3.2 | Bearings With a Rolling Element Fault (Ball)

Figure 14 highlights the influence of varying the number of poles (M) on the MPMFs formats for bearings exhibiting a rolling element fault. The dataset consists of 16 distinct vibration signals from bearings exhibiting rolling element faults, each reconstructed using the proposed MP approach with different numbers of poles as $M = 70$, $M = 50$ and $M = 30$. The colour spectrum, transitioning from blue to red, represents the frequencies of the poles for each case ($M = 70$, $M = 50$, $M = 30$). The impact of the variation in the number of poles is apparent as the MPMF format changes for each case. Significantly, a

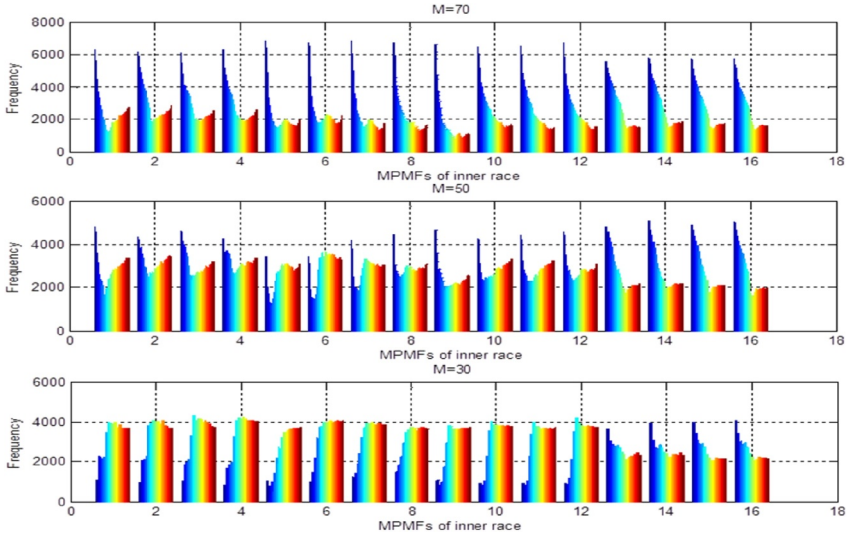

FIGURE 13 | Impact of the number of poles (M) on MPMF formats in the inner race case ($M = 70$, $M = 50$, $M = 30$).

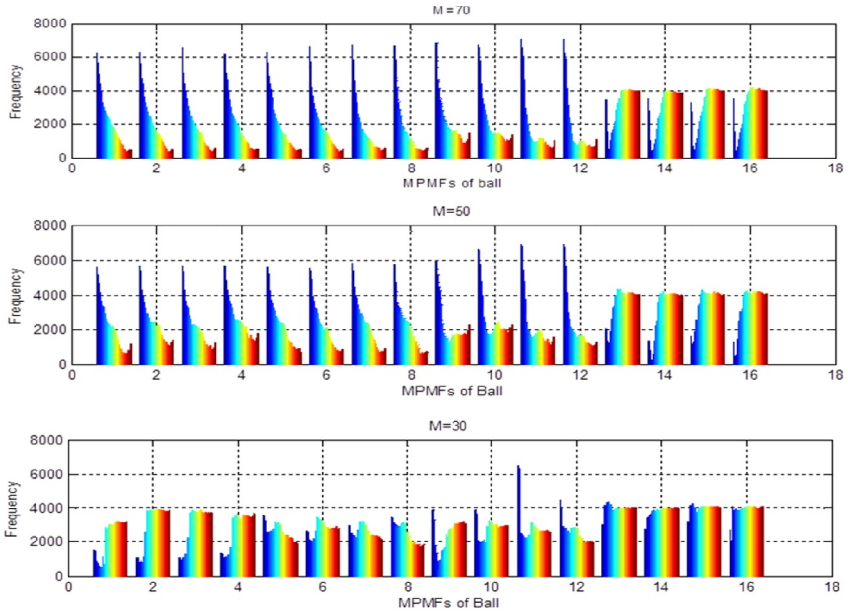

FIGURE 14 | Impact of the number of poles (M) on MPMF Formats in the bearings exhibiting a rolling element fault case ($M = 70$, $M = 50$, $M = 30$).

distinct resemblance in the forms of the first 4 MPMFs becomes evident, underscoring the consistency across these signals, particularly in bearings with a rolling element fault diameter of 0.007″.

This consistent pattern extends to MPMFs 5–8, representing bearings exhibiting a rolling element fault of 0.014″, and persists in the subsequent MPMFs (9–12 and 13–16) corresponding to bearings exhibiting a rolling element fault of 0.021″ and 0.028″, respectively. These notable resemblances in the MPMF forms emphasise the consistency across these signals. The shapes of the MPMFs adeptly capture and differentiate the vibrational characteristics associated with different numbers of poles for bearings with a rolling element fault.

3.3.3 | For a Healthy Bearing

Figure 15 shows the impact of varying the number of poles (M) on the MPMFs formats for a healthy bearing. The original database comprises four distinct vibration signals from healthy bearings, each reconstructed using the proposed MP approach with different numbers of poles: $M = 70$, $M = 50$ and $M = 30$. The colour spectrum, transitioning from blue to red, represents the frequencies of the poles for each case ($M = 70$, $M = 50$, $M = 30$). The influence of the variation in the number of poles is evident as the MPMF format changes for each case with a segment length (SL = 250). Each MPMF encapsulates the inherent characteristics of the corresponding healthy bearing vibration signal. Remarkably, a clear similarity in MPMF forms emerges, emphasising the consistency across these signals. This uniformity in the MPMF shapes highlights the robustness of the proposed approach, ensuring reliability and accuracy in capturing the vibrational characteristics of healthy bearings across different pole configurations.

3.3.4 | For Bearings With an Outer Race Fault

Figure 16 visualises the impact of varying the number of poles (M) on the formats of MPMFs for bearings with an Outer race fault. The original dataset comprises 28 distinct vibration signals from bearings with an outer race fault, each reconstructed using the proposed PM approach with different numbers of poles: $M = 70$, $M = 50$ and $M = 30$, along with a segment length (SL = 250). The colour spectrum, transitioning from blue to red, represents the frequencies of the poles for each case ($M = 70$, $M = 50$, $M = 30$). A noticeable distinction in the forms of the first four MPMFs emerges, emphasising the consistency across these signals, exemplified by bearings with an outer race fault diameter of 0.014″. This distinctive pattern extends to MPMFs 5–8, 9–12, 13–16, reflecting bearings with an outer race fault of 0.007″ under different accelerometer positions (centred for MPMFs 5–8, opposite for MPMFs 9–12, orthogonal for MPMFs 19–16), and persists in the subsequent MPMFs (17–20, 21–24, 25–28), corresponding to bearings with outer race faults of 0.021″ under different accelerometer positions (centred for MPMFs 17–20, opposite for MPMFs 21–24, orthogonal for MPMFs 25–28). These distinct resemblances in the forms of the MPMFs underscore the consistency across these signals. The shapes of the MPMFs effectively capture and distinguish the vibrational characteristics associated with different numbers of poles for bearings with an outer race fault, providing a reliable and comprehensive analysis.

3.4 | Exploring the Impact of Window Size on the Forms of MPMF

3.4.1 | Healthy Bearing

Figure 17 illustrates the impact of varying segment length (SL) on the MPMF formats for a healthy bearing. The original

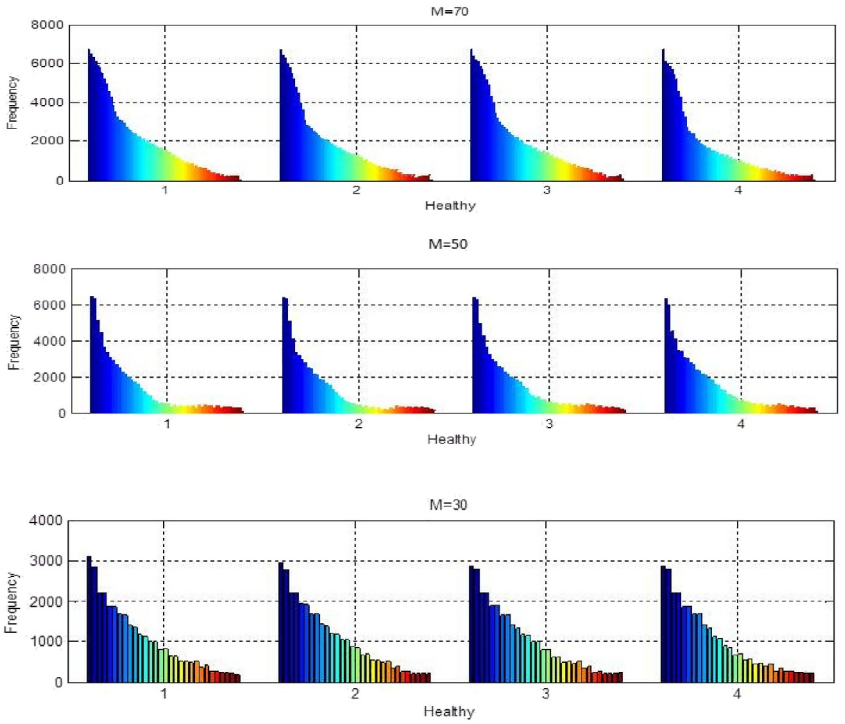

FIGURE 15 | Impact of the number of poles (M) on MPMF formats in healthy bearing case ($M = 70$, $M = 50$, $M = 30$).

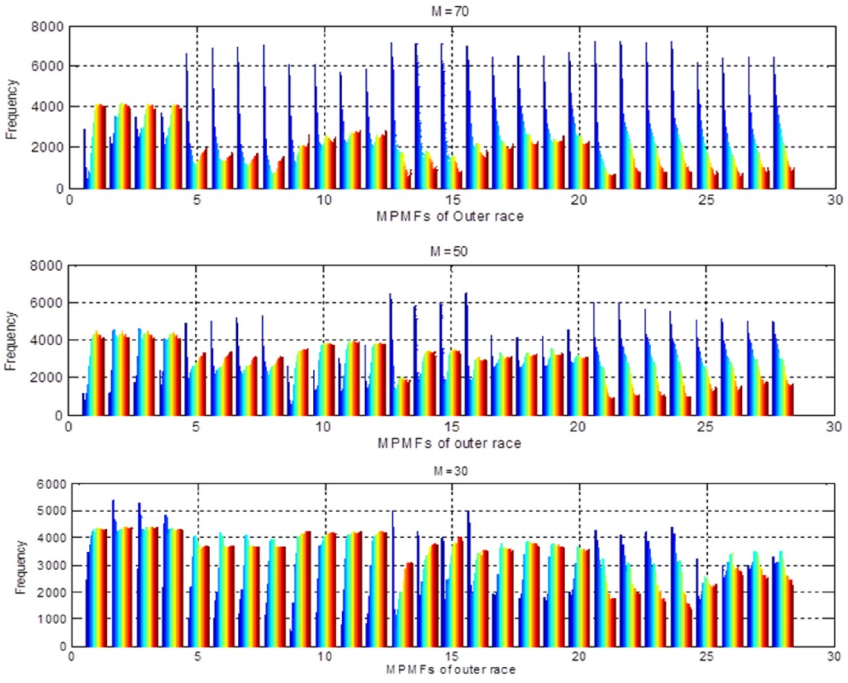

FIGURE 16 | Impact of the number of poles (M) on MPMF formats in the outer race case ($M = 70$, $M = 50$, $M = 30$).

database comprises four distinct vibration signals from healthy bearings, each reconstructed using the proposed PM approach with $M = 100$ poles, and the scenario includes cases with two segment lengths (SL = 300, SL = 400).

The colour spectrum, transitioning from blue to red, represents the frequencies of the poles ranging from 1 to 100 poles. The influence of the variation in segment length is evident as the MPMF format changes for each case. Each MPMF encapsulates the inherent characteristics of the corresponding healthy bearing vibration signal. Remarkably, a clear similarity in MPMF forms emerges, emphasising the consistency across these signals. This uniformity in the MPMF shapes highlights the robustness of the proposed approach, ensuring reliability and accuracy in capturing the vibrational characteristics of healthy bearings across different segment lengths.

3.4.2 | For Bearings With an Inner Race

Figure 18 demonstrates the impact of varying segment length on the MPMFs formats for bearings exhibiting an inner race fault. The dataset comprises 16 distinct vibration signals from bearings with an inner race fault, each reconstructed using the proposed Matrix Pencil approach with a constant number of poles $M = 100$, and the scenario includes cases with two segment lengths (SL = 300, SL = 400). The colour spectrum, transitioning from blue to red, represents the frequencies of the poles ranging from 1 to 100 poles. The effect of the varying segment length is evident as the format of MPMF changes for each case. Notably, the variation in bearings with an inner race fault diameter of 0.007″ is most noticeable in the first four MPMFs. This consistent pattern prolongs to MPMFs 5–8, reflecting bearings with an inner race fault of 0.028″, and continues in the subsequent MPMFs (9–12 and 13–16), corresponding to bearings with inner race faults of 0.014″ and 0.021″, respectively. These distinct resemblances in the forms of the MPMFs highlight the consistency across these signals. The shapes of the MPMFs effectively capture and distinguish the vibrational characteristics associated with different segment lengths for bearings with an inner race fault.

3.4.3 | For Bearings With an Outer Race

Figure 19 showcases the influence of varying segment length on the MPMFs formats for bearings with an outer race fault. The dataset comprises 28 unique vibration signals from bearings with an outer race fault. Each signal is reconstructed

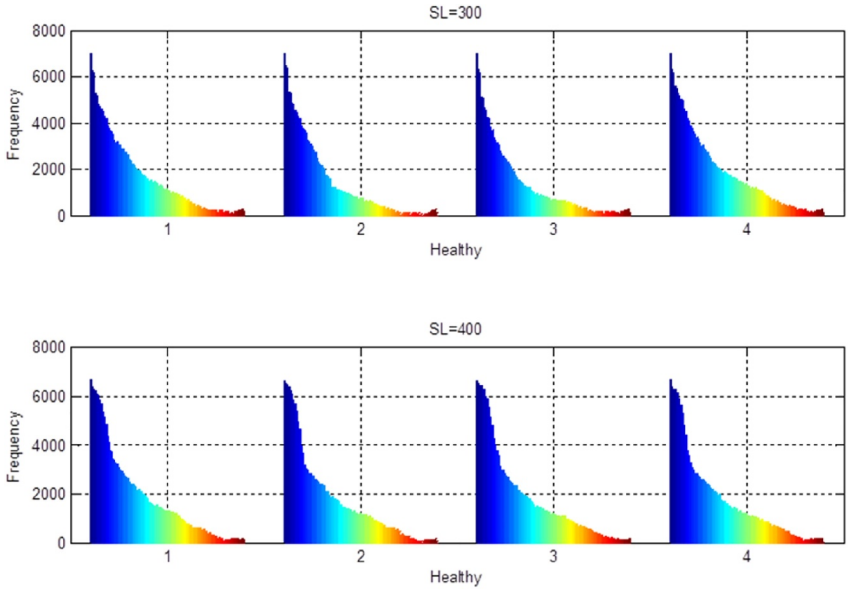

FIGURE 17 | Impact of the window size on the forms of MPMF in the healthy bearing case (SL = 300, SL = 400).

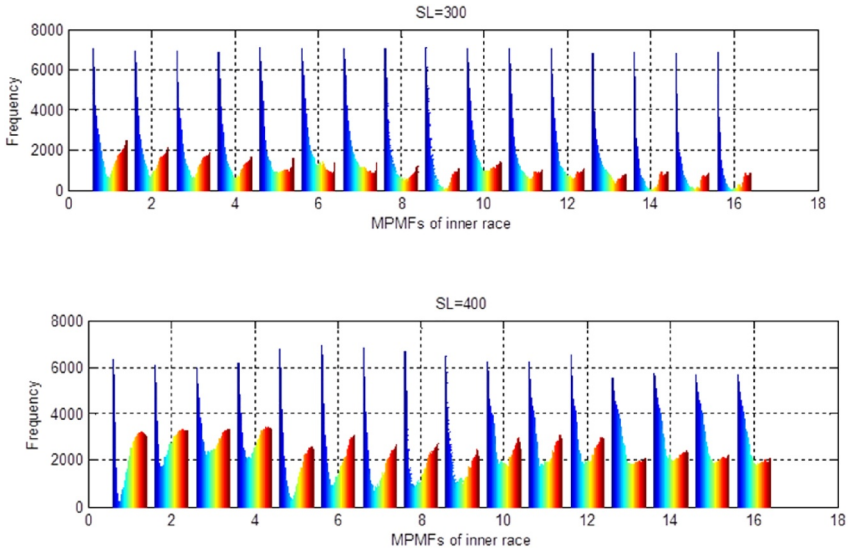

FIGURE 18 | Impact of the window size on the forms of MPMF in the inner race case (SL = 300, SL = 400).

using the Matrix Pencil approach to maintain a constant number of poles ($M = 100$) and explore two segment lengths (SL = 300, SL = 400). The colour spectrum, shifting from blue to red, corresponds to the frequencies of the poles ranging from 1 to 100 poles. The impact of the changing segment length is evident as the format of MPMF adjusts for each case. Clear distinctions emerge in the forms of the initial four MPMFs, underlining the consistency across these signals, particularly notable in bearings with an outer race fault diameter of 0.014″. This characteristic pattern extends through MPMFs 5–8, 9–12 and 13–16, representing bearings with an outer race fault of 0.007″ in various accelerometer positions (centred for MPMFs 5–8, opposite for MPMFs 9–12, orthogonal for MPMFs 19–16). This consistency persists in subsequent MPMFs (17–20, 21–24, 25–28), corresponding to bearings with outer race faults of 0.021″ in different accelerometer positions (centred for MPMFs 17–20, opposite for MPMFs 21–24, orthogonal for MPMFs 25–28). The distinct resemblances in the MPMFs underscore the consistency across these signals, effectively capturing and differentiating the vibrational characteristics associated with varying segment lengths for bearings with an outer race fault.

3.4.4 | Bearings With a Rolling Element Fault (Ball)

Figure 20 depicts the influence of varying segment length on the MPMFs formats for bearings exhibiting a fault in the rolling element. The dataset comprises 16 unique vibration signals from bearings with an inner race fault, each reconstructed using the proposed MP approach, maintaining a constant number of poles ($M = 100$) and exploring two segment lengths (SL = 300, SL = 400). The colour spectrum, transitioning from blue to red, corresponds to the frequencies of the poles ranging from 1 to 100 poles. The impact of the changing segment length is evident as the MPMF format adapts for each case. Notably, variations in bearings with an inner race fault diameter of 0.007″ are most pronounced in the initial four MPMFs. This consistent pattern extends to MPMFs 5–8, portraying bearings with an inner race fault of 0.028″, and persists in the subsequent MPMFs (9–12 and

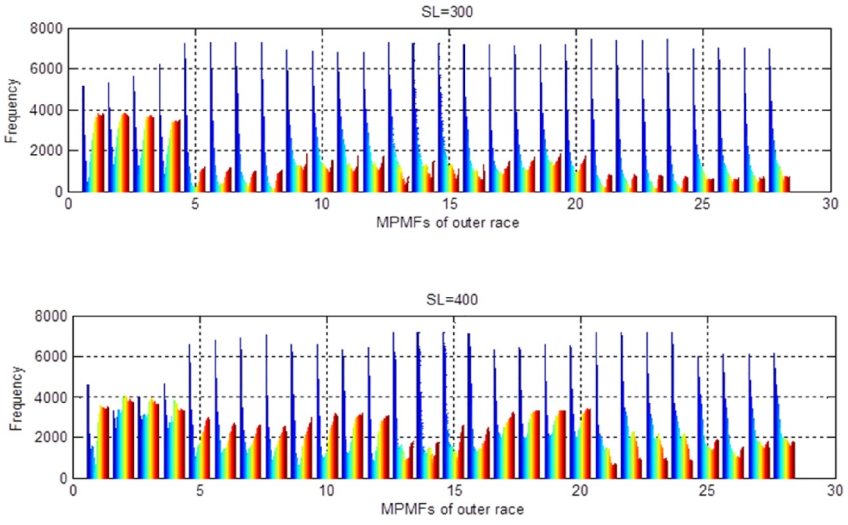

FIGURE 19 | Impact of the window size on the forms of MPMF in the outer race case (SL = 300, SL = 400).

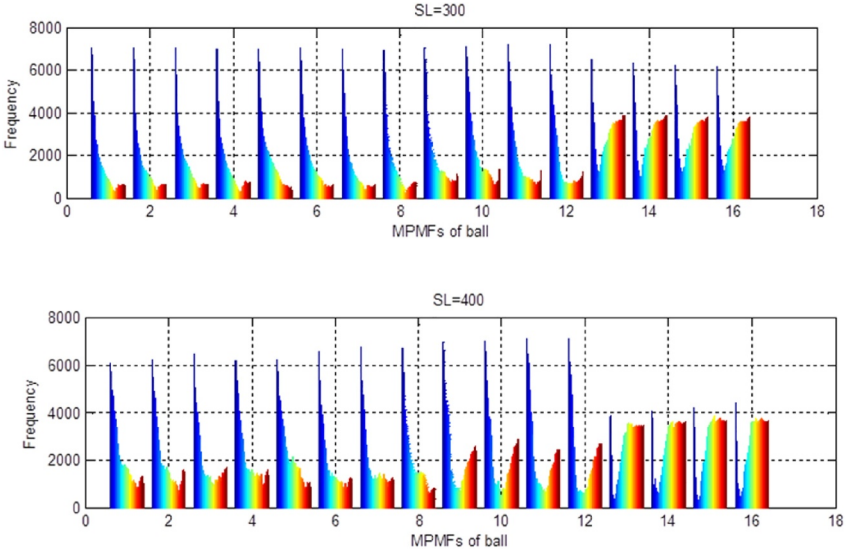

FIGURE 20 | Impact of the window size on the forms of MPMF in the bearings with a rolling element fault case (SL = 300, SL = 400).

13–16), representing bearings with inner race faults of 0.014″ and 0.021″, respectively. These distinct resemblances in the forms of the MPMFs emphasise the consistency across these signals. The shapes of the MPMFs proficiently capture and differentiate the vibrational characteristics associated with different segment lengths for bearings with a rolling element fault.

Envelope Analysis was applied solely for signal interpretation and fault characterisation (see Figure 21). The resulting envelope spectra for the healthy bearing, inner race fault, outer race fault, and ball fault cases enabled the identification of characteristic fault frequencies and validated the vibratory behaviour of the raw signals. Furthermore, this method requires manual selection of filter bands tailored to known fault frequencies, which reduces its level of automation and limits its generalisability to varying machines or operating conditions.

In contrast, the proposed MPMF approach is fully data-driven and does not rely on predefined fault frequencies. It extracts dominant spectral features directly from the vibration signal using the Matrix Pencil Method, enabling consistent and automated feature generation. This distinction is visually supported in Figure 12, which presents examples of MPMF shapes associated with different bearing conditions. These spectral representations reveal clear structural differences between classes details that are not as easily distinguishable through traditional envelope spectra alone.

4 | Localisation of the Defected Component Based on Multilayer Perceptron Neural Networks

In the last few decades, artificial intelligence approaches have been the focus of most studies aiming to automate defect diagnostics in rotating machinery. These can be used as defect detectors and fault classifiers to aid in diagnosis and reduce the need for human intervention [36]. In the course of our research, the classification of bearing faults was investigated using multilayer perceptron neural networks. Although the MPMF profiles effectively capture and differentiate the vibrational characteristics associated with different bearing conditions and have demonstrated their effectiveness in enhancing the impact of a localisation of the defective component, facilitating easier detection and localisation, they may not furnish comprehensive details about the fault. Understanding fault classes is crucial for assessing the severity of bearing faults, and an inverse problem approach using a Multilayer Perceptron is proposed to address this. Neural networks, particularly MLPs [37, 38], have shown versatility across various engineering applications, and their integration with reliability analysis methods, such as the PINN-FORM approach, tackles the challenges posed by partial differential equations [39]. MLPs are effective in approximating relationships in nonlinear systems, serving as surrogate models for capturing fundamental input-output correlations. By training the MLP on input-output pairs, it can predict input causes based on observed outputs, a valuable approach for complex systems where traditional techniques struggle. The

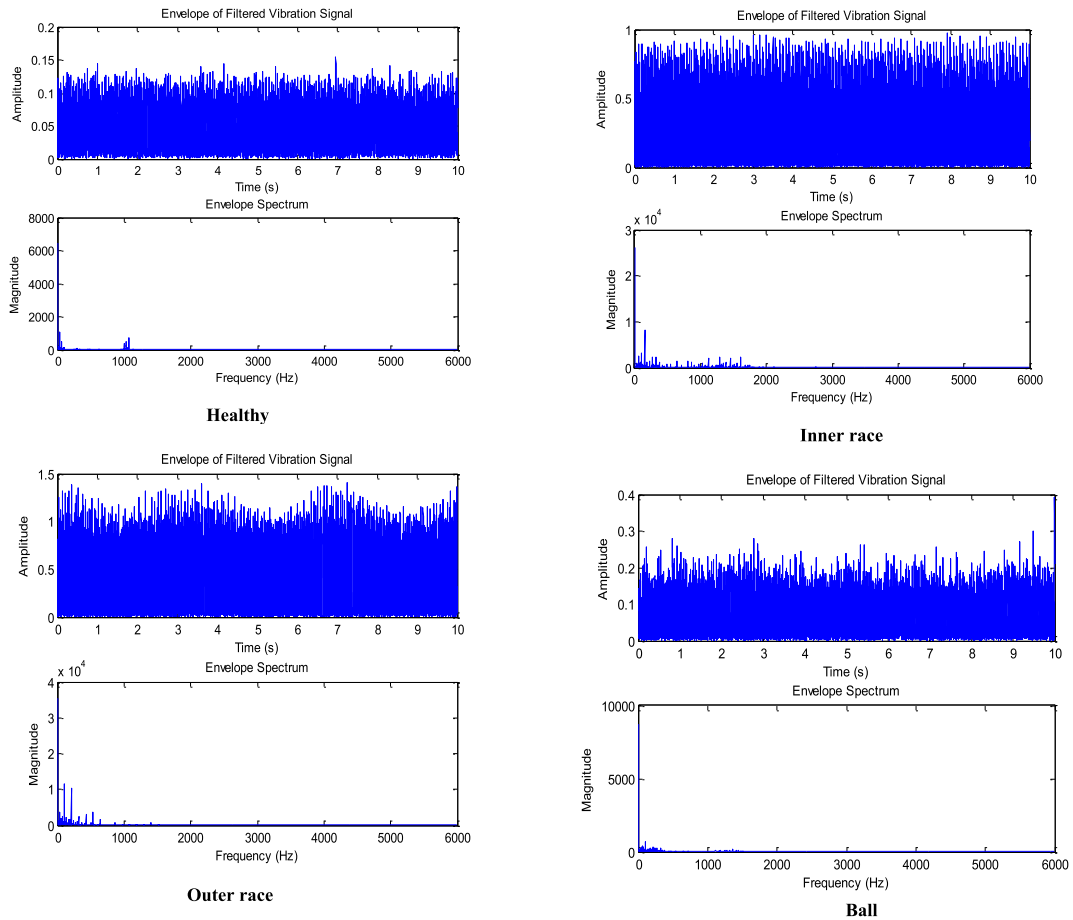

FIGURE 21 | Envelope spectrum of a vibration signal for (healthy, inner race, outer race, ball).

network's architecture, including the number of layers and neurons, alongside data quality, is critical for accuracy. The MLP used in this study employs the Levenberg–Marquardt optimisation technique to adjust its weights and biases. Previous research [40–42] confirms the effectiveness of MLPs in fault detection and localisation. The MLP architecture utilised here comprises an input layer with 75 neurons, a hidden layer of 25 neurons, and a single-neuron output layer as illustrated in Figure 22. The dataset links MPMF features to fault types, including healthy bearings, outer and inner race faults, and rolling element faults. From the 64 available examples, 85% were used for training and 15% for testing. Root Mean Square (RMS) error was used to assess the model's generalisation. Eight databases with Matrix Pencil Mean Frequencies generated under different segment lengths (SL = 250 to SL = 300) and poles ($M = 100$ to $M = 30$) were employed to evaluate fault classification performance, measured in terms of accuracy, sensitivity, specificity, precision and G-mean, which are defined below.

The classification accuracy is defined as follows:

$$\mathrm{Acc} = \frac{\mathrm{TP} + \mathrm{TN}}{\mathrm{TP} + \mathrm{TN} + \mathrm{FP} + \mathrm{FN}}. \tag{20}$$

Sensitivity indicates the ability to identify a positive result when a fault exists and is defined as follows:

$$\mathrm{Sens} = \frac{\mathrm{TP}}{\mathrm{TP} + \mathrm{FN}}. \tag{21}$$

Specificity reflects the capacity to achieve a negative result when no fault is present and is defined as follows:

$$\mathrm{Spec} = \frac{\mathrm{TN}}{\mathrm{TN} + \mathrm{FP}}. \tag{22}$$

Precision represents the proportion of predicted positive cases that are actually positive and is defined as follows:

$$\mathrm{Prec} = \frac{\mathrm{TP}}{\mathrm{TP} + \mathrm{FP}}. \tag{23}$$

The G-mean is the geometric mean of sensitivity and specificity and is defined as follows:

$$\mathrm{G_{mean}} = \sqrt{\mathrm{Sens} * \mathrm{Prec}}. \tag{24}$$

In the above formula's TP denotes True Positive, TN represents True Negative, FP stands for False Positive and FN indicates False Negative. These metrics collectively offer insights into the efficacy of fault classification algorithms. Table 2 illustrates various outcomes obtained from the Multilayer Perceptron classifier across eight distinct databases. Although the database is constrained in all utilised datasets (1–8), a notable pattern emerges in databases 3 (SL = 250, $M = 50$) and 7 (SL = 300, $M = 50$), where sensitivity demonstrates an exceptional rate of 100%. This signifies a remarkable capacity to accurately detect positive instances of bearing faults. Furthermore, specificity tends towards an impressive rate of 100%, indicating a high likelihood of correctly identifying negative instances when the bearing is in good condition. Additionally, the classifier exhibits precision levels of 100%, underscoring its ability to predict positive instances with remarkable accuracy. The G-Mean rate serves as a pivotal metric in assessing the classifier's performance, particularly in discerning the classification efficacy of positive cases, notwithstanding the correct identification of negative cases. Remarkably, the G-Mean value attains a robust rate of 100%, indicative of well-classified positive instances.

Conversely, in the remaining databases (1, 2, 4, 5, 8), although sensitivity varies between 66% and 100%, it consistently

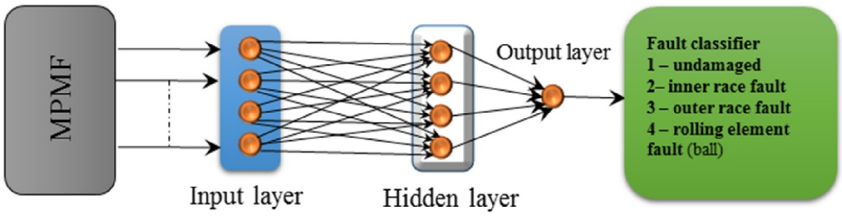

FIGURE 22 | Schematic diagram of a fault classifier grounded on MLP network with diverse input of MPMF.

TABLE 2 | Performance evaluation criteria results of MLP classifier across 8 databases.

	Evaluation criteria				
Databases (SL, *M*)	**Accuracy**	**Sensitivity**	**Specificity**	**Precision**	**G-mean**
Databases1 (SL = 250, $M = 100$)	66.66	100	57.14	40	63.24
Databases2 (SL = 250, $M = 70$)	77.77	66.66	83.333	66.66	66.66
Databases3 (SL = 250, $M = 50$)	100	100	100	100	100
Databases4 (SL = 250, $M = 30$)	88.88	100	85.71	66.66	81.65
Databases5 (SL = 300, $M = 100$)	88.88	66.66	100	100	81.65
Databases6 (SL = 300, $M = 70$)	88.9	66.66	100	100	0.8165
Databases7 (SL = 300, $M = 50$)	100	100	100	100	100
Databases8 (SL = 300, $M = 30$)	77.8	100	71.42	50	70.71

demonstrates a notable capacity to capture positive instances of bearing faults. Similarly, specificity fluctuates between 57.14% and 100%, denoting varying degrees of accuracy in identifying negative instances. The classifier's precision spans between 40% and 100%, indicating a moderate ability to predict positive instances. The G-Mean rate fluctuates between 63.42% and 100% in these databases, highlighting moderate performance in classifying positive instances. Finally, the accuracy, representing the proportion of correctly classified cases, ranges between 63.24% and 81.65%, demonstrating the classifier's efficacy across these datasets. These performance measurements underscore the classifier's robustness and effectiveness, particularly evident in databases 3 and 7. Despite limitations in dataset size, the classifier consistently demonstrates notable capabilities in fault detection and classification accuracy.

In the context of evaluating the confusion matrix for four classes attained by the MLP neural network classifier, the classifier underwent rigorous training and testing procedures using eight distinct databases. Notably, the third database corresponds to conditions characterised by a segment length of 250 and a number of poles (M) set to 50, while the seventh database reflects conditions with SL = 300 and $M = 50$. The comprehensive analysis of the obtained results, as depicted in Figures 23 and 24, showcases the confusion matrices for the third and seventh databases, respectively. Each cell within these matrices corresponds to a specific combination of predicted and true class labels. Attaining 100% accuracy indicates the absence of misclassifications across all classes. The diagonal elements of the confusion matrices denote the true positive counts for each class. In this context, these values are maximised, underscoring the classifier's precise identification of instances within each class. Conversely, the absence of off-diagonal elements signifies the absence of misclassifications, highlighting the classifier's remarkable capability to accurately assign instances to their respective classes. This exceptional performance underscores the MLP neural network's robustness in discerning intricate patterns and features within the dataset, facilitating precise classification across all classes. In the remaining databases (1, 2, 4, 5, 8), the confusion matrix results are as duplicated in Figure 25.

To simulate real-world operating conditions, Additive White Gaussian Noise (AWGN) was added to the MPMF features in the datasets, specifically Databases 3 (SL = 250, $M = 50$) and Databases 7 (SL = 300, $M = 50$). The results are given in Table 3. The power of the noise (Pn) was calculated relative to the power of the MPMF features (Ps) according to Equation (25):

$$\mathrm{SNR} = 10 \log \frac{\mathrm{Ps}}{\mathrm{Pn}} \tag{25}$$

These results demonstrate the strong noise resilience of the proposed MPMF-MLP approach. Both datasets maintained 100% classification accuracy at SNR levels down to 0 dB and +3 dB, indicating robust performance under mild to moderate noise conditions. However, as the SNR decreased further into negative values (e.g., −1 dB and −5 dB), a reduction in accuracy was observed, in both Databases7, and Databases3 where accuracy dropped to 77.7% at −1 dB. Despite this degradation, the method still achieved notable accuracy even at −5 dB, which reflects realistic industrial noise scenarios. Overall, these findings confirm that the proposed approach remains effective even in challenging noisy environments, supporting its potential applicability in practical bearing fault detection systems where ambient and structural noise can significantly mask fault signatures.

The effectiveness of the MPMF method depends on key parameters such as the number of poles (M) and segment length (SL), which influence the resolution and robustness of extracted features. A higher M improves spectral resolution but increases noise sensitivity, whereas a lower M may result in information loss. Similarly, a shorter SL enhances time localisation but

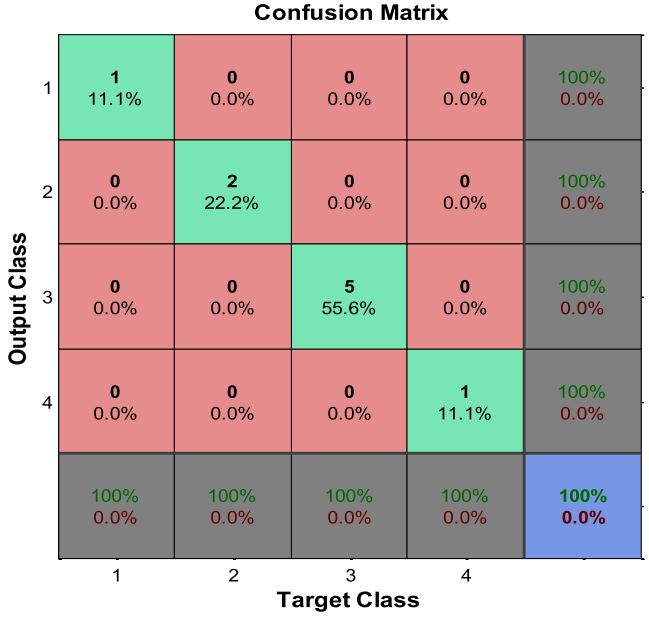

FIGURE 23 | Confusion matrix for MLP classifier (case of SL = 250, $M = 50$).

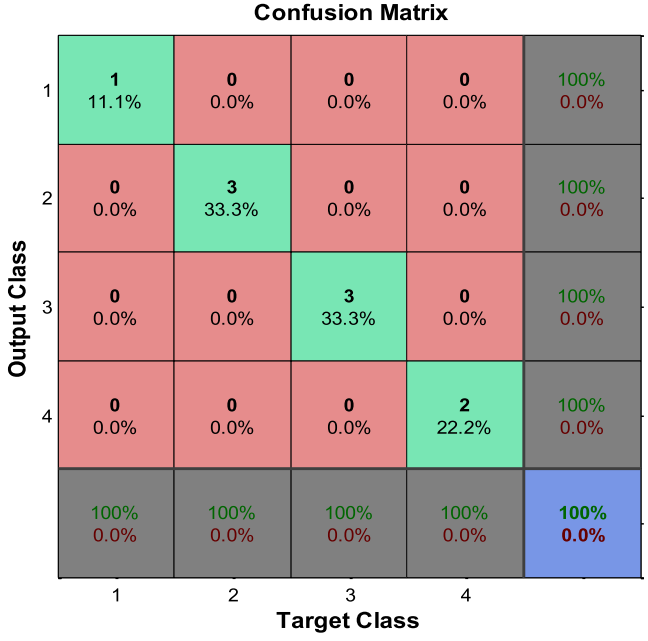

FIGURE 24 | Confusion matrix for MLP classifier (case of SL = 300, $M = 50$).

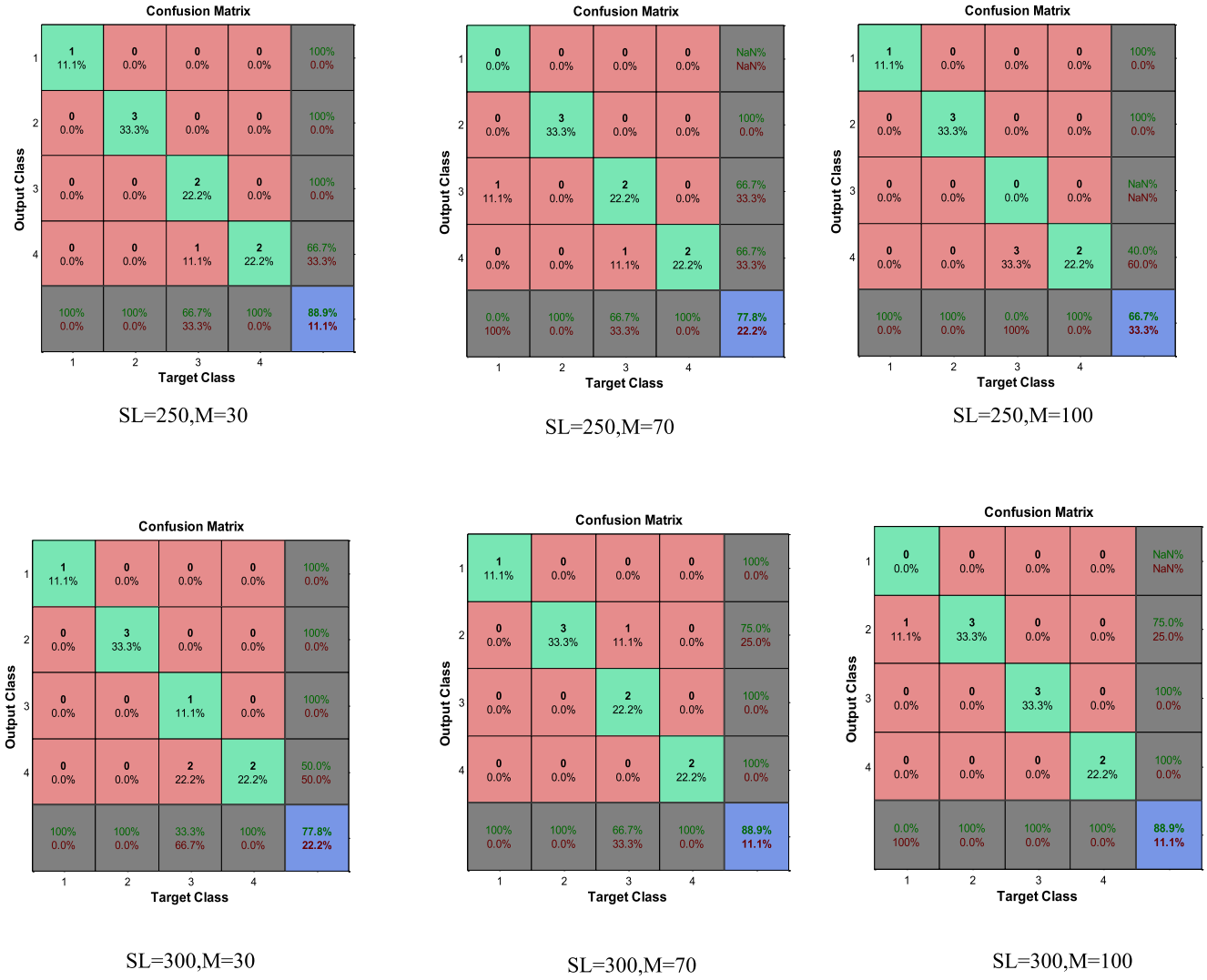

FIGURE 25 | Confusion matrix for MLP classifier (case of SL = 300, $M = 50$).

TABLE 3 | Presents the classification accuracies achieved under various SNR levels, ranging from +3 dB to −5 dB.

	Accuracy					
Databases (SL, *M*)	**0 dB**	**1 dB**	**2 dB**	**3 dB**	**−1 dB**	**−5 dB**
Databases3 (SL = 250, $M = 50$)	100	100	100	100	77.77	88.9
Databases7 (SL = 300, $M = 50$)	100	100	100	100	77.8	88.9

reduces frequency resolution, while a longer SL provides greater spectral precision at the cost of potentially averaging out transient fault features. To optimise these parameters, a grid search was conducted, and classification accuracy was analysed across different settings. As shown in Figures 23 and 24, the third database (SL = 250, $M = 50$) and the seventh database (SL = 300, $M = 50$) achieved 100% classification accuracy, with confusion matrices demonstrating zero misclassifications. This confirms that the selected values effectively capture fault characteristics while ensuring model stability. The comparison of accuracy between the proposed MPMF-MLP method and other recent works highlights the diversity of methodologies utilised in bearing fault diagnosis. For instance, methods such as Linear Discriminant Analysis combined with Neural Networks achieved an accuracy of 98.7% [43], while Multi-domain Entropy paired with Random Forest yielded an accuracy of 94.4% [44]. Principal Component Analysis integrated with Long Short-Term Memory and Random Forest achieved an accuracy of 96.04% [45], and Multigrained Scanning with Cascade Forest resulted in a range of 96.99%–98.54% [46]. Additionally, Genetic Algorithm with Random Forest and DWT-ENV-Random Forest reached impressive accuracies of 99.5% [47] and 99.53% [48], respectively.

In contrast, the novel MPMF-MLP approach, which combines Matrix Pencil Mean Frequency analysis with a Multilayer Perceptron neural network, stands out by achieving perfect accuracy at 100%. This integration not only outperforms existing

methodologies but also signifies a breakthrough in the field of fault diagnosis in bearing systems. Recent work by Alonso-González et al. [49] applied Envelope Analysis on the CWRU dataset and combined it with machine learning classifiers to diagnose bearing faults. Their study achieved 100% accuracy with Decision Tree (Fine Tree) and k-NN (Fine k-NN) also 94.4% accuracy with the Kernel Naïve Bayes classifier. Although Envelope Analysis has proven effective, it requires careful selection of frequency bands and pre-processing using techniques like the Fast Kurtogram. In contrast, MPMF extracts spectral information directly from vibration signals without requiring additional band selection, making it more adaptable across different conditions.

The practical advantages of the proposed MPMF-MLP method over traditional approaches such as Wavelet Transform (WT) and Empirical Mode Decomposition (EMD) lie in its ability to extract frequency components directly from the vibration signal based on the system's dynamic behaviour, without relying on predefined basis functions. In contrast, WT operates by decomposing the signal into sub bands, which may limit its adaptability to varying signal characteristics. Similarly, while EMD adaptively decomposes signals into intrinsic mode functions (IMFs), it often suffers from mode mixing and a lack of mathematical rigour, which can affect the consistency and interpretability of the extracted features. Although this study does not include a direct experimental comparison, previous works ([50, 51]) have evaluated WT and EMD on the CWRU bearing dataset. The classification accuracies, reproduced in Figure 26, serve as benchmarks. Despite achieving similar accuracy to WPT + LDA, the proposed MPMF-MLP approach provides a more physically meaningful representation of the signal, offering greater generalisation capability for real-world applications. To further evaluate the trade-off between classification performance and computational efficiency, a comparative study was conducted using the same MPMF feature vectors across three classifiers: Multilayer Perceptron (MLP), Support Vector Machine (SVM) and k-Nearest Neighbours (k-NN). Seven datasets with varying signal lengths (SL) and numbers of poles (M) were constructed, and each model was implemented in MATLAB 2013b using identical training and testing splits. For each case, both classification accuracy and average inference time per sample were measured. The results, summarised in Table 4, show that the MLP consistently achieved the highest or equal accuracy, reaching 100% in Databases 3 and 7, while the maximum accuracies obtained by SVM and k-NN were 81.25% and 87.50%, respectively. However, the MLP required slightly more computational time, with inference times ranging from 0.01028 to 0.02198 s per sample, compared to 0.00193–0.00638 s for SVM and 0.01474–0.05004 s for k-NN. These findings highlight the strength of the MLP model in terms of accuracy, particularly for lower-dimensional MPMF representations, while also demonstrating the advantage of SVM and k-NN in terms of computational speed. This analysis confirms that the choice of model should be guided by the specific application context whether prioritising accuracy, as in offline diagnostics, or computational efficiency, as required in real-time industrial monitoring.

Also, we conducted a supplementary experiment using hidden Markov models (HMMs) on the same MPMF feature vectors. The resulting classification accuracy was approximately 6.25%, which is significantly lower than that achieved by the proposed MPMF-MLP approach. This low performance is primarily due to a mismatch between the nature of the features and the modelling strengths of HMMs. Specifically, HMMs are designed to model temporal sequences and state transitions, such as in time-series analysis, where the order and dependency between observations are essential. In contrast, MPMF features are compact, frequency-based descriptors that summarise the spectral content of signal segments without encoding any temporal progression. As such, they do not provide the sequential structure required by HMMs to construct effective state-transition models, thereby explaining the poor classification results. On the other hand, the proposed MPMF-MLP method leverages the dominant spectral information directly, without relying on assumptions about temporal states or transitions. This makes it more suitable, flexible, and accurate for bearing fault detection tasks, particularly under noisy conditions.

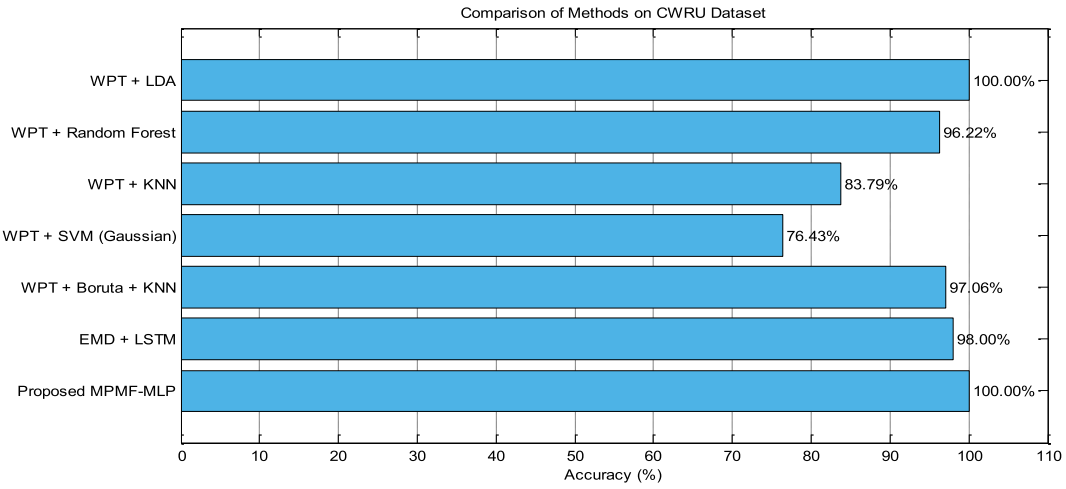

FIGURE 26 | Classification accuracy of various methods on the CWRU dataset.

TABLE 4 | Comparison of classification accuracy and inference time for MLP, SVM and k-NN classifiers using MPMF features across seven datasets.

	MLP		SVM		KNN	
Databases (SL, *M*)	**Accuracy (%)**	**Inference time(s)**	**Accuracy (%)**	**Inference time(s)**	**Accuracy (%)**	**Inference time(s)**
Databases1 (SL = 250, $M = 100$)	66.66	0.02198	56.25	0.00638	62.50	0.05004
Databases2 (SL = 250, $M = 70$)	77.77	0.01160	56.25	0.00198	68.75	0.01580
Databases3 (SL = 250, $M = 50$)	100	0.01080	62.5	0.00193	87.50	0.01474
Databases4 (SL = 250, $M = 30$)	88.88	0.01217	68.75	0.00208	81.25	0.01735
Databases5 (SL = 300, $M = 100$)	88.88	0.01028	50	0.00202	50	0.01576
Databases6 (SL = 300, $M = 70$)	88.9	0.01059	81.25	0.00198	75.00	0.01707
Databases7 (SL = 300, $M = 50$)	100	0.01154	43.75	0.00223	75.00	0.01849

5 | Discussion on Dataset Limitations and Generalisation

Although the proposed approach has been validated using the Case Western Reserve University bearing dataset, we acknowledge that this dataset, although widely used in fault diagnosis research, may not fully capture the diverse conditions encountered in real-world industrial environments. Factors such as variable load conditions, fluctuating rotational speeds, and different bearing types can influence the vibration characteristics and impact the generalisability of the model. Reference [15] demonstrated that MPM performs effectively in noisy environments when used in conjunction with pre-processing techniques such as Wavelet De-noising and Wiener Filtering. In this work, we enhance the robustness of MPMF features under high noise levels. Furthermore, the stability of MPMF features under varying load conditions and external disturbances such as temperature fluctuations and electromagnetic interference remains insufficiently investigated and is addressed in this study. Although MPMF effectively captures dominant spectral characteristics, factors such as load-induced frequency shifts or signal distortions from electromagnetic interference may influence its robustness in real-world applications. Because our method is data-driven and relies on spectral feature extraction through MPMF, it is inherently adaptable to different datasets, provided that the model is trained with representative data.

6 | Conclusion

In conclusion, the proposed approach addresses critical challenges in machinery condition monitoring and fault diagnosis, particularly for induction motors, by leveraging the strengths of advanced signal processing and machine learning techniques. Vibration analysis remains an indispensable tool for predictive maintenance, as it enables the detection, collection, and analysis of vibration signals to assess machinery conditions accurately. This paper introduces a novel technique for automatic bearing condition assessment, integrating the Matrix Pencil method and a Multilayer Perceptron (MLP) neural network. The first methodology focuses on signal processing using the Matrix Pencil method, which effectively decomposes machinery vibration signals into frequency vectors, capturing dynamic spectral components. Through meticulous aggregation, the Matrix Pencil Mean Frequency (MPMF) vector emerges as a robust representation that encapsulates the collective frequency characteristics of the signal. This novel feature offers a clearer and more insightful spectrum for characterising machinery faults, enhancing fault detection and condition monitoring by providing a comprehensive view of the signal's behaviour. The second methodology involves the application of an MLP classifier, which validates the effectiveness of the MPMF vector as a novel feature for bearing fault detection. Achieving a fault classification rate of 100%, the classifier demonstrates a high level of accuracy while autonomously identifying defective components, reducing the dependency on human expertise and minimising the potential for misinterpretation. Experimental validation conducted using a specialised test rig, along with comparisons to recent literature, underscores the robustness and practical applicability of the proposed method. By addressing limitations associated with raw data, inefficient feature extraction, and the need for dimensionality reduction, this approach provides a reliable and efficient solution for fault diagnosis in industrial settings. The findings hold significant potential for advancing the state of the art in machinery condition monitoring, contributing to more reliable and efficient industrial systems and reinforcing the importance of integrating advanced signal processing with machine learning for predictive maintenance. Future work can explore the integration of digital modelling techniques, such as finite element simulations and digital twin technology, to reduce reliance on extensive physical experiments. These approaches can generate synthetic fault signals, enabling rapid validation and refinement of fault diagnosis models before real-world deployment. By leveraging

digitisation, the proposed method can be further enhanced for broader industrial applications. Additionally, predicting the remaining useful life (RUL) of bearings is a critical aspect of predictive maintenance. Although this study focuses on fault detection, future research can extend the MPMF framework to track fault progression over time. By integrating time-series degradation analysis and machine learning models (e.g., Recurrent Neural Networks [RNNs]), the method can be adapted for data-driven RUL estimation. This enhancement would enable proactive maintenance strategies, reducing unplanned downtime and optimising operational efficiency. By incorporating these advancements, the proposed method has the potential to evolve into a comprehensive predictive maintenance solution, bridging the gap between fault detection and lifetime prognosis in industrial machinery.

Author Contributions

Abderrzak Laib: conceptualization, formal analysis, investigation, methodology, software, writing – original draft. **Saida Dahmane:** conceptualization, supervision, writing – review and editing. **Yacine Terriche:** conceptualization, supervision, writing – review and editing. **Chun-Lien Su:** conceptualization, supervision, writing – review and editing. **Hafiz Ahmed:** conceptualization, project administration, supervision, writing – review and editing. **Zakaria Chedjara:** conceptualization, supervision, writing – review and editing.

Acknowledgements

During the preparation of this work, the authors used ChatGPT exclusively to assist with language refinement and readability. All AI-generated content was carefully reviewed, edited and verified by the authors, who take full responsibility for the accuracy, integrity and originality of the final manuscript.

Conflicts of Interest

The authors declare no conflicts of interest.

Data Availability Statement

The authors confirm that the data supporting the findings of this study are available within the article.

References

1. M. F. Yakhni, S. Cauet, A. Sakout, et al., "Variable Speed Induction Motors' Fault Detection Based on Transient Motor Current Signatures Analysis: Aa Review," *Mechanical Systems and Signal Processing* 184 (2023): 1–22, https://doi.org/10.1016/j.ymssp.2022.109737.

2. C. Lessmeier, J. K. Kimotho, D. Zimmer, and W. Sextro, "Condition Monitoring of Bearing Damage in Electromechanical Drive Systems by Using Motor Current Signals of Electric Motors: A Benchmark Data Set for Data-Driven Classification," *Third European Conference of the PHM Society (PHME16)* 3, no. 1 (2016): 152–156, https://doi.org/10.36001/phme.2016.v3i1.1577.

3. R. A. Rahman, M. F. Erikyatna, and A. F. Hery, "Study on Predictive Maintenance of V-Belt in Milling Machines Using Machine Learning Study on Predictive Maintenance of V-Belt in Milling Machines Using," *Machine Learning* 6, no. 2 (November 2022): 85–94, https://doi.org/10.17977/um016v6i22022p085.

4. A. Picot, Z. Obeid, J. Régnier, S. Poignant, O. Darnis, and P. Maussion, "Statistic-Based Spectral Indicator for Bearing Fault Detection in Permanent-Magnet Synchronous Machines Using the Stator Current," *Mechanical Systems and Signal Processing* 46, no. 2 (2014): 424–441, https://doi.org/10.1016/j.ymssp.2014.01.006.

5. M. Ye, J. Zhang, and J. Yang, "Bearing Fault Diagnosis Under Time-Varying Speed and Load Conditions via Observer-based Load Torque Analysis," *Energies* 15, no. 10 (2022): 3532, https://doi.org/10.3390/en15103532.

6. A. Allouche, E. Etien, T. Doget, et al., "A PLL Based Mechanical Faults Detection in PMSM at Variable Speed," *IFAC-PapersOnLine* 51, no. 24 (2018): 1445–1451, https://doi.org/10.1016/j.ifacol.2018.09.534.

7. M. A. Jamil and S. Khanam, "Fault Classification of Rolling Element Bearing in Machine Learning Domain," *International Journal of Acoustics and Vibration* 27, no. 2 (2022): 77–90, https://doi.org/10.20855/ijav.2022.27.21829.

8. S. Tang, S. Yuan, and Y. Zhu, "Data Preprocessing Techniques in Convolutional Neural Network Based on Fault Diagnosis Towards Rotating Machinery," *IEEE Access* 8 (2020): 149487–149496, https://doi.org/10.1109/ACCESS.2020.3012182.

9. A. Rai and S. H. Upadhyay, "Bearing Performance Degradation Assessment Based on a Combination of Empirical Mode Decomposition and k-Medoids Clustering," *Mechanical Systems and Signal Processing* 93 (2017): 16–29, https://doi.org/10.1016/j.ymssp.2017.02.003.

10. J. Singh, A. K. Darpe, and S. P. Singh, "Bearing Damage Assessment Using Jensen-Rényi Divergence Based on EEMD," *Mechanical Systems and Signal Processing* 87, no. April (2017): 307–339, https://doi.org/10.1016/j.ymssp.2016.10.028.

11. T. Han, C. Liu, W. Yang, and D. Jiang, "Deep Transfer Network With Joint Distribution Adaptation: A New Intelligent Fault Diagnosis Framework for Industry Application," *ISA Transactions* 97 (2020): 269–281, https://doi.org/10.1016/j.isatra.2019.08.012.

12. S. Tang, S. Yuan, and Y. Zhu, "Convolutional Neural Network in Intelligent Fault Diagnosis Toward Rotatory Machinery," *IEEE Access* 8 (2020): 86510–86519, https://doi.org/10.1109/ACCESS.2020.2992692.

13. L. I. Gliga, D. Popescu, and H. Chafouk, "Fault Detection Using State Estimation and Machine Current Signature Analysis," *UPB Scientific Bulletin, Series C: Electrical Engineering and Computer Science* 83, no. 3 (2021): 47–58.

14. R. N. Toma and J. M. Kim, "Bearing Fault Classification of Induction Motors Using Discrete Wavelet Transform and Ensemble Machine Learning Algorithms," *Applied Science* 10, no. 15 (2020): 5251, https://doi.org/10.3390/APP10155251.

15. K. C. Deekshit Kompella and G. V. Madhav, "An Improved Matrix Pencil Method Based Bearing Fault Detection in Three Phase Induction Motor," in *IEEE International Conference on Computing, Power and Communication Technologies (GUCON 2020)* (2020), 51–56, https://doi.org/10.1109/GUCON48875.2020.9231196.

16. V. Venkatasubramanian, R. Rengaswamy, K. Yin, and S. N. Kavuri, "A Review of Process Fault Detection and Diagnosis Part I: Quantitative Model-Based Methods," *Computers & Chemical Engineering* 27, no. 3 (2003): 293–311, https://doi.org/10.1016/S0098-1354(02)00160-6.

17. Y. Lei, B. Yang, X. Jiang, F. Jia, N. Li, and A. K. Nandi, "Applications of Machine Learning to Machine Fault Diagnosis: A Review and Roadmap," *Mechanical Systems and Signal Processing* 138 (2020): 106587, https://doi.org/10.1016/j.ymssp.2019.106587.

18. D. Wu, J. Wang, H. Wang, et al., "An Automatic Bearing Fault Diagnosis Method Based on Characteristics Frequency Ratio," *Sensors (Switzerland)* 20, no. 5 (2020): 1–12, https://doi.org/10.3390/s20051519.

19. P. Kamat, P. Marni, L. Cardoz, et al., "Bearing Fault Detection Using Comparative Analysis of Random Forest, ANN, and Autoencoder Methods," *Lecture Notes in Networks and Systems* 204, no. June (2021): 157–171, https://doi.org/10.1007/978-981-16-1089-9_14.

20. S. chikkam and S. Singh, "Condition Monitoring and Fault Diagnosis of Induction Motor Using DWT and ANN," *Arabian Journal for*

Science and Engineering 48, no. 5 (2023): 6237–6252, https://doi.org/10.1007/s13369-022-07294-3.

21. Y. Terriche, M. U. Mutarraf, A. Laib, et al., "A Resolution-Enhanced Sliding Matrix Pencil Method for Evaluation of Harmonics Distortion in Shipboard Microgrids," *IEEE Transactions on Transportation Electrification* 6, no. 3 (September 2020): 1290–1300, https://doi.org/10.1109/tte.2020.3020820.

22. Y. Terriche, A. Laib, A. Lashab, C.-L. Su, J. M. Guerrero, and J. C. Vasquez, "A Frequency Independent Technique to Estimate Harmonics and Interharmonics in Shipboard Microgrids," *IEEE Transactions on Smart Grid* 13, no. 2 (March 2022): 888–899, https://doi.org/10.1109/TSG.2021.3128554.

23. I. Bouaissi, A. Laib, A. Rezig, et al., "Frequency Bearing Fault Detection in Non-Stationary State Operation of Induction Motors Using Hybrid Approach Based on Wavelet Transforms and Pencil Matrix," *Electrical Engineering* 106, no. 4 (2024): 4397–4413, https://doi.org/10.1007/s00202-023-02235-1.

24. T. K. Sarkar and O. Pereira, "Using the Matrix Pencil Method to Estimate the Parameters of a Sum of Complex Exponentials," *IEEE Antennas and Propagation Magazine* 37, no. 1 (1995): 48–55, https://doi.org/10.1109/74.370583.

25. M. H. Chia and A. M. Khambadkone, "Subcycle Voltage Dip Classification Using Matrix Pencil Method With Ellipse Fitting Algorithm," *IEEE Transactions on Industry Applications* 51, no. 2 (2015): 1660–1668, https://doi.org/10.1109/TIA.2014.2347455.

26. T. K. Sarkar, S. Park, J. Koh, and S. M. Rao, "Application of the Matrix Pencil Method for Estimating the SEM (Singularity Expansion Method) Poles of Source-Free Transient Responses From Multiple Look Directions," *IEEE Transactions on Antennas and Propagation* 48, no. 4, (2000): 612–618, https://doi.org/10.1109/8.843676.

27. X. Xu, M. Zhao, and J. Lin, "Detecting Weak Position Fluctuations From Encoder Signal Using Singular Spectrum Analysis," *ISA Transactions* 71 (November 2017): 440–447, https://doi.org/10.1016/j.isatra.2017.09.001.

28. C. Yi, Y. Lv, Z. Dang, H. Xiao, and X. Yu, "Quaternion Singular Spectrum Analysis Using Convex Optimization and Its Application to Fault Diagnosis of Rolling Bearing," *Measurement* 103 (June 2017): 321–332, https://doi.org/10.1016/j.measurement.2017.02.047.

29. M. Zhao and X. Jia, "A Novel Strategy for Signal Denoising Using Reweighted SVD and Its Applications to Weak Fault Feature Enhancement of Rotating Machinery," *Mechanical Systems and Signal Processing* 94 (September 2017): 129–147, https://doi.org/10.1016/j.ymssp.2017.02.036.

30. P. Bonizzi, J. M. H. Karel, O. Meste, and R. L. M. Peeters, "Singular Spectrum Decomposition: A New Method for Time Series Decomposition," *Advances in Adaptive Data Analysis* 6, no. 4 (2014): 1450011, https://doi.org/10.1142/S1793536914500113.

31. Y. Mao, M. Jia, and X. Yan, "A New Bearing Weak Fault Diagnosis Method Based on Improved Singular Spectrum Decomposition and Frequency-Weighted Energy Slice Bispectrum," *Measurement* 166 (2020): 108235: ISSN 0263-2241, https://doi.org/10.1016/j.measurement.2020.108235.

32. K. Zheng, T. Li, Z. Su, J. Wen, B. Zhang, and Yi Zhang, "Faults Diagnosis of Rolling Bearings Based on Shift Invariant K-Singular Value Decomposition With Sensitive Atom Nonlocal Meansenhancement," *Measurement* 135 (2019): 836–851: ISSN0263 2241, https://doi.org/10.1016/j.measurement.2018.12.043.

33. G. Wu, T. Yan, G. Yang, H. Chai, and C. Cao, "A Review on Rolling Bearing Fault Signal Detection Methods Based on Different Sensors," *Sensors* 22, no. 21 (2022): 8330, https://doi.org/10.3390/s22218330.

34. C. Malla and I. Panigrahi, "Review of Condition Monitoring of Rolling Element Bearing Using Vibration Analysis and Other Techniques," *Journal of Vibration Engineering & Technologies* 7, no. 4 (2019): 407–414, https://doi.org/10.1007/s42417-019-00119-y.

35. "Bearing Data Center," Case Western Reserve University, http://csegroups.case.edu/bearingdatacenter/pages/welcome-casewestern-reserve-university.

36. J. S. R. Nkuna, *Vibration Condition Monitoring and Fault Classification of Rolling Element Bearings Utilising Kohonen's Self-Organising Maps*. Thèse de Doctorat (Université de Vaal de Technologie, 2006).

37. C. Fan, Y. Peng, Y. Shen, et al., "Variable Scale Multilayer Perceptron for Helicopter Transmission System Vibration Data Abnormity Beyond Efficient Recovery," *Engineering Applications of Artificial Intelligence* 133, no. Part B (2024): 108184: ISSN 0952-1976, https://doi.org/10.1016/j.engappai.2024.108184.

38. A. Mystkowski, A. Wolniakowski, A. Idzkowski, et al., "Measurement and Diagnostic System for Detecting and Classifying Faults in the Rotary Hay Tedder Using Multilayer Perceptron Neural Networks," *Engineering Applications of Artificial Intelligence* 133, no. Part E (2024): 108513: ISSN 0952-1976, https://doi.org/10.1016/j.engappai.2024.108513.

39. Z. Meng, Q. Qian, M. Xu, Bo Yu, A. R. Yıldız, and S. Mirjalili, "PINN-FORM: A New Physics-Informed Neural Network for Reliability Analysis With Partial Differential Equation," *Computer Methods in Applied Mechanics and Engineering* 414 (2023): 116172, https://doi.org/10.1016/j.cma.2023.116172.

40. A. Laib, M. Melit, B. Nekhoul, K. Kerroum, and K. Drissi, "A New Hybrid Approach Using Time-Domain Reflectometry Combined With Wavelet and Neural Network for Fault Identification in Wiring Network," in *2016 8th International Conference on Modelling, Identification and Control (ICMIC)* (2016), 290–295, https://doi.org/10.1109/ICMIC.2016.7804125.

41. A. Laib, M. Melit, B. Nekhoul, K. Kerroum, and K. E. Drissi, "A New Hybrid Approach Using Time-Domain Reflectometry Combined With Wavelet and Neural Network for Fault Identification in Wiring Network," in *2016 8th International Conference on Modelling, Identification and Control (ICMIC)* (2016), 290–295.

42. A. Laib, Y. Terriche, M. Melit, et al., "Enhanced Artificial Intelligence Technique for Soft Fault Localization and Identification in Complex Aircraft Microgrids," *Engineering Applications of Artificial Intelligence* 127, no. Part B (2023): 107289, https://doi.org/10.1016/j.engappai.2023.107289.

43. J. J. Saucedo-Dorantes, I. Zamudio-Ramirez, J. Cureno-Osornio, R. A. Osornio-Rios, and J. A. Antonino-Daviu, "Condition Monitoring Method for the Detection of Fault Graduality in Outer Race Bearing Based on Vibration-Current Fusion, Statistical Features and Neural Network," *Applied Sciences* 11, no. 17 (2021): 8033, https://doi.org/10.3390/app11178033.

44. J. Tian, L. Liu, F. Zhang, Y. Ai, R. Wang, and C. Fei, "Multi-Domain Entropy-Random Forest Method for the Fusion Diagnosis of Inter-Shaft Bearing Faults With Acoustic Emission Signals," *Entropy* 22, no. 1 (2020): 57, https://doi.org/10.3390/e22010057.

45. H. Zhou, L. Cheng, L. Teng, and H. Sun, "Bearing Fault Diagnosis Based on RF-PCA-LSTM Model," in *2021 2nd Information Communication Technologies Conference (ICTC)* (IEEE, May 2021), 278–282, https://doi.org/10.1109/ICTC51749.2021.9441578.

46. X. Qin, D. Xu, X. Dong, X. Cui, and S. Zhang, "The Fault Diagnosis of Rolling Bearing Based on Improved Deep Forest. Shock and Vibration. The Fault Diagnosis of Rolling Bearing Based on Improved Deep Forest," *Shock and Vibration* (2021): 1–13, https://doi.org/10.1155/2021/9933137.

47. R. N. Toma, A. E. Prosvirin, and J. M. Kim, "Bearing Fault Diagnosis of Induction Motors Using a Genetic Algorithm and Machine Learning Classifiers," *Sensors* 20, no. 7 (2020): 1884, https://doi.org/10.3390/s20071884.

48. S. Dahmane, F. Berrabah, M. Defdaf, S. Salah, "Diagnosis and Monitoring Method for Detecting and Localizing Bearing Faults," *Indonesian Journal of Electrical Engineering and Informatics (IJEEI)* 12, no. 1, (March 2024): 1–14: ISSN: 2089-3272, https://doi.org/10.52549/ijeei.v12i1.4612.

49. M. Alonso-González, V. G. Díaz, B. L. Pérez, B. C. P. G-Bustelo, and J. P. Anzola, "Bearing Fault Diagnosis With Envelope Analysis and Machine Learning Approaches Using CWRU Dataset," *IEEE Access* 11 (2023): 57796–57805, https://doi.org/10.1109/ACCESS.2023.3283466.

50. W. Li, L. Wang, P. Lu, and L. Hua, "Bearing Fault Diagnosis Research Based on Empirical Mode Decomposition and Deep Learning," in *2020 35th Youth Academic Annual Conference of Chinese Association of Automation (YAC)* (2020), 32–37, https://doi.org/10.1109/YAC51587.2020.9337677.

51. A. S. Maliuk, Z. Ahmad, and J.-M. Kim, "A Technique for Bearing Fault Diagnosis Using Novel Wavelet Packet Transform-Based Signal Representation and Informative Factor LDA," *Machines* 11, no. 12 (2023): 1080, https://doi.org/10.3390/machines11121080.